Density Functional Theory for the Hubbard-Holstein model

PERNILLA HELMER | DEPARTMENT OF PHYSICS | LUND UNIVERSITY

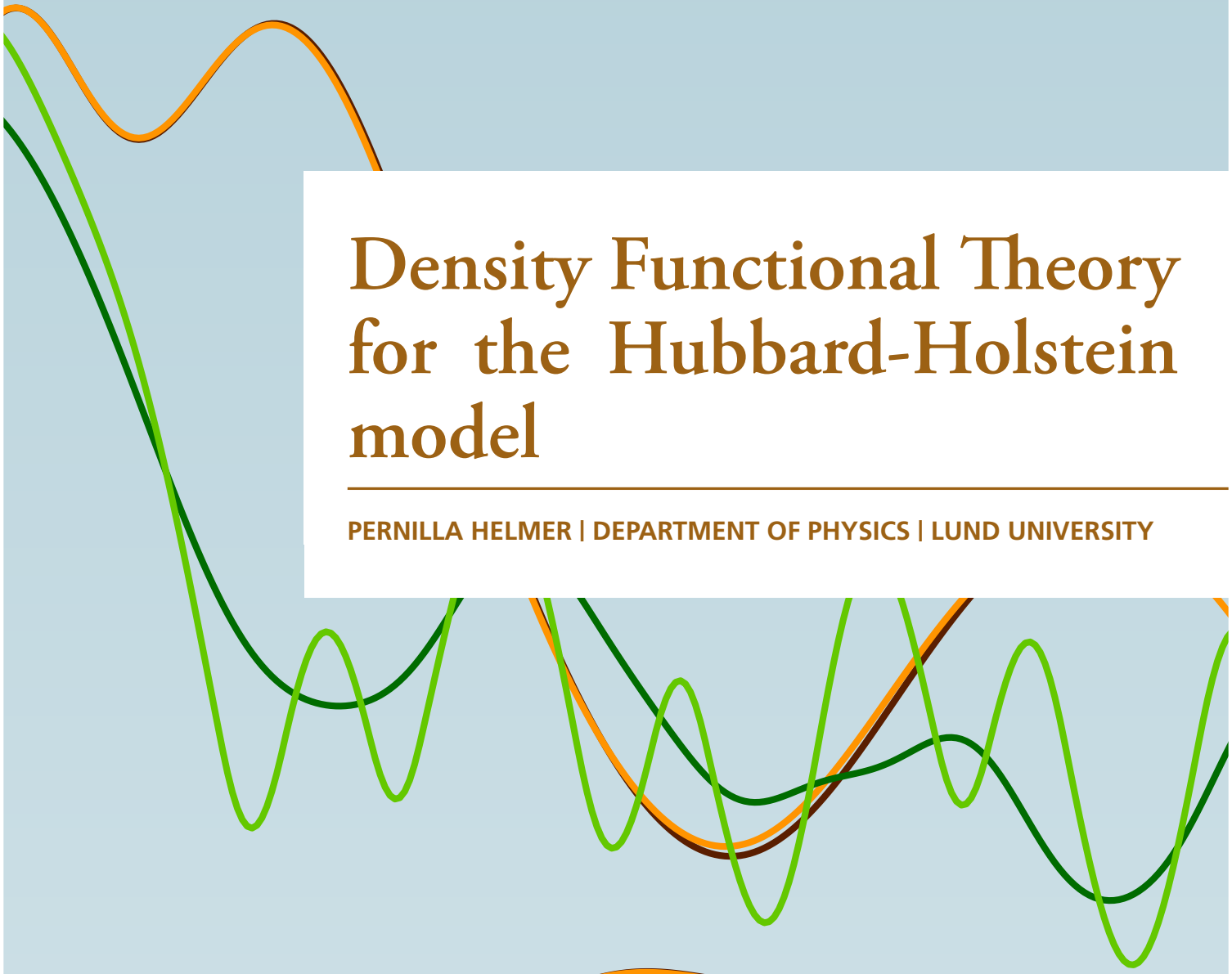

Division of Mathematical Physics
Department of Physics
Faculty of Science
Lund University

February 2018

Density Functional Theory for the Hubbard-Holstein model

Pernilla Helmer

LUND
UNIVERSITY

A Thesis Submitted for the Degree of Master of Science
60 credits
Supervisor: Prof. Claudio Verdozzi
Co-supervisor: Emil Viñas Boström

Division of Mathematical Physics
Department of Physics
Faculty of Science

February 2018

February 2018

Lund mPh-18/01

Pernilla Helmer
Division of Mathematical Physics
Department of Physics
Faculty of Science
Lund University
P.O. Box 118
S-221 00 Lund, Sweden

Acknowledgements

First and foremost I would like to thank my supervisor Claudio Verdozzi for always being avaliable and for the support he has given me when things didn't turn out the way they were supposed to. I would also like to thank my co-supervisor Emil Vinas Boström who has been very helpful and friendly and never lost patience with me when I just wouldn't get things, or if he did, at least he never let me know. I am grateful to Philipp Werner for providing the DMFT-code used during this thesis work, and to Carl-Olof Almbladh for making it compile. And finally, I want to express my gratitude to Sebastian Pfaff for always keeping me company, for the pretty frontpage and beamer templates and for fixing LaTeXwhenever, in standard LaTeX-fashion, it would refuse to behave, and to Tim Almqvist, for all the little things he figured out for me when I failed to figure them out for myself, and for teaching me about computers.

Abstract

The physics of interacting many-body systems is a very complex and challenging subject. Therefore one in general needs to use simplified models and approximate methods for studying these systems theoretically. In this work we study the exchange-correlation (xc) potential for the Hubbard-Holstein (HH) model for the application of Density Functional Theory (DFT) to the same.

The Hohenberg-Kohn theorem and the two sets of Kohn-Sham equations are derived for the HH-model extending a procedure outlined in previous work. The xc-potentials for the fermions and bosons respectively are then derived analytically as functions of the density n and phononic displacement x for a single HH-site in contact with a heat bath, generalizing the procedure for the pure Hubbard model. The potential for the HH-site is found to have a smaller gap at half filling than for the Hubbard model, due to a rescaling of the effective electron-electron interaction. It also has an additional term linear in $(n-1)$. The xc-potentials are used to study two simple systems, an Andersson impurity dimer and a four-site chain of HH-sites. The results are compared to those of an exact solution and to the Hartree-Fock (HF) solution. For the dimer the DFT-method performs consistently better than the HF-method, while the results for the chain are more ambiguous.

However, the central result of this thesis is to produce xc-potentials for an infinitely coordinated Bethe lattice, using Dynamical Mean Field Theory (DMFT). The potentials for a small but representative set of interaction parameters are presented and compared to the analytical potential. The potentials are similar in that they do not exhibit much structure, and they behave very similarly far from half filling. Close to half filling they show more differences, as the analytic potential is always discontinuous around half filling while the potential attained via DMFT is only discontinuous for large electron-electron interactions.

Contents

List of Abbreviations

DFT - Density Functional Theory
xc - Exchange-Correlation
HH - Hubbard-Holstein
BSC theory - Bardeen–Cooper–Schrieffer theory
DMFT - Dynamical Mean Field Theory
HF - Hartree-Fock
LF - Lang Firsov
HK - Hohenberg-Kohn
KS - Kohn-Sham
LDA - Local Density Approximation
TDDFT - Time Dependent Density Functional Theory
ALDA - Adiabatic Local Density Approximation
DOS - Density Of States
AIM - Andersson Impurity Model
ED - Exact Diagonalization
CTQMC - Continous Time Quantum Monte Carlo

1 Introduction

The physics of many-body systems is very complex and poses some of the major challenges in modern physics. The cause of this complexity is that in most many-body systems of interest, each particle interacts with every other particle, resulting in a problem which expands rapidly in size and quickly becomes too complicated to solve exactly. In order to treat these complicated systems, many different approaches have been taken, and multiple approximation methods have been developed. One which is commonly employed is density functional theory (DFT), which was developed during the -60's by Hohenberg, Kohn and Sham [10, 16], and for which Kohn got the Nobel prize in chemistry in 1998. The basic idea of DFT is to remodel the interacting system as an auxiliary, non-interacting one with the same particle density as the fully interacting system. This is done by subjecting the auxiliary system to an effective potential which gives rise to the correct particle density. It can be shown that the particle density is enough to uniquely define any expectation value of the original system, and thus the full many-body wavefunction does in principle not need to be evaluated, if the particle density can be found. These ideas are presented in more detail in section 1.2.

In DFT, the primary challenge is moved from finding the interacting many-body wave function into finding the effective potential of the auxiliary system, or rather the part of this effective potential referred to as the exchange correlation (xc) potential. This quantity is defined as the contribution which describes the exchange and correlation effects of the full system, or more simply: the complicated part. This is, just as finding the full many-body wave function, an in principle impossible task. For certain types of systems good approximations of this potential have however been developed, and DFT can be used to accurately predict some properties of actual, physical systems, such as inter-atomic distances.

Another tool that can be used to gain a better understanding of many-body physics is simplified model systems. These can be studied both in order to investigate qualitative behaviour which can be compared to experimental results, as well as to compare different approximation schemes to exact solutions, and to each other. For example, an extensive amount of work has been done on the Hubbard model [13, 14, 8], which is a very simple lattice model that only accounts for next-neighbour hopping and an on-site electron-electron Coulomb interaction, U. This makes it useful for studying systems with strong electron-electron interactions, so called strongly correlated systems. This thesis considers another rather simple lattice model, called the Hubbard-Holstein (HH) model [25]. This models combines the Hubbard-model with another model, the Holstein model [11], which describes an on-site interaction between fermions and bosons. The Holstein model thus accounts for the interaction between electrons and lattice vibrations (phonons). To study the HH-model would then be interesting in order to gain better understanding of systems which experience both strong correlation effects and strong electron-phonon interactions. The HH-model is described in

more detail in section 1.1.

Besides fundamental scientific curiosity, a convincing motivation for studying the HH-model is the wish to gain better understanding of superconductivity, in particular at high temperature. In 1957 Bardeen, Cooper and Schrieffer formulated the BCS-theory, which explains the physics of conventional superconductors [3]. This theory shows that at low enough temperatures electrons will form Cooper pairs, which are bosonic quasi particles consisting of two electrons of opposite spin, indirectly attracted to each other through interactions with the lattice. It also succeeds in describing other properties of superconducting materials, although it falls short in explaining high temperature superconductors, discovered in 1986 [4]. These are materials that are superconducting at temperatures higher than predicted by the BSC-theory, and they are still not well understood. There is experimental evidence that lattice vibrations plays a role also in high temperature superconductors, and that these materials exhibit strong correlation effects. For example strong isotope effects and peculiar electron dispersion has been observed in certain high temperature superconductors [9, 18]. The HH-model is the simplest model possible which accounts for both strong electron-electron repulsion and electron-phonon interactions. Extracting the xc-potential for the HH-model could thus help give insight to the behaviour of high temperature superconductors, by providing the possibility of an approximate description of them using DFT.

Another area where the model is of direct interest is ultra cold atoms. In these systems atoms are cooled to extremely low temperatures ($T \ll 1$ K) and trapped by an optical lattice. These setups permit to adjust and fine tune parameters which can not be easily changed in conventional solids, such as the band width and on-site interaction. This type of experiments could therefore be a very direct way of testing theoretical predictions of the model.

This masters project is, however, not directly concerned with any experimental applications. Rather, it presents a sample of the HH-model xc-potential for a small set of different electron-electron and electron-phonon interactions, as well as an analytical xc-potential for the special case of a single HH-site system coupled to a heat bath. This analytical potential is obtained via an extension of the work done for the Hubbard model in [24, 26, 22], and it is used to simulate a simple system.

In this section the theoretical background for the thesis is presented, describing the model and the methods used to solve it, and in the next section the theoretical work done during this thesis is presented. In 2.1 we show that the concept of DFT makes sense for the HH-model by generalizing the proof in [23], and in section 2.2 the xc-energy for the HH-model is separated from the total energy, as this quantity is needed for the data analysis in section 4.3. We then develop an analytical expression for the xc-potential of a single HH-site in contact with a heat bath. This analytical potential is obtained as an extension of the treatment of [24, 26] and [22], by considering the electron-phonon interaction of the HH-model in addition to the electron-electron interaction of the pure Hubbard model. This is presented in section 2.3. The phonons are found to rescale

the effective electron repulsion, so that for phonon couplings similar in strength to the electronic interaction U, the effective electron interaction can even become attractive.

The theory concerning the simulations performed during this project is presented in section 3 along with the specific systems that were simulated. The analytical potential developed in section 2.3 is used to study the behaviour of a dimer consisting of one HH-site and one non-interacting site serving as the heat bath. The results, presented in section 4.1, are compared to the exact solution and also to the Hartree-Fock (HF) solution, which is briefly described in section 1.2.3. It is found that the analytical xc-potential in general performs better than the HF-potential, but not always.

The main goal of the thesis however was to attain the xc-potential using a more realistic model than the single-site dimer in contact with the heat bath. This was done with a code which uses Dynamical Mean Field Theory (DMFT) to find the local Green's function for a Bethe lattice (see section 1.3.5), from which the xc-potential can be derived [1]. The DMFT method and the concept of Green's functions are discussed in section 1.3. The procedure is a generalization to that of [15] where the same was done for the Hubbard model in 3D. However, these simulations require a vast amount of computational effort to converge. Therefore we focused on attaining data for a small but representative set of parameters U and g, presented in section 4.3. In section 4.4 the results are discussed and the analytical and DMFT-results are compared to each other.

Finally section 5 provides a short summary of the work that has been done during the course of this thesis project, as well as an outlook with suggestions on further developments on the topic.

1.1 The Hubbard-Holstein model

The Hubbard-Holstein (HH) Hamiltonian is a model lattice Hamiltonian. It describes a many-body system of electrons tightly bound to the lattice sites, accounting for local interactions between the electrons and between electrons and on-site lattice vibrations. The electrons are tightly bound in the sense that they can only hop between next neighbour sites. The atomic orbitals of the lattice sites are used as the fermionic basis states and the bosonic number states as the phononic basis. Defining the fermionic and bosonic annihilation and creation operators acting at a lattice site i as $\mathrm{a}_{i,\sigma}/\mathrm{a}^\dagger_{i,\sigma}$ and $\mathrm{b}_i/\mathrm{b}^\dagger_i$ respectively, where $\sigma = \uparrow / \downarrow$ denotes spin, the HH-Hamiltonian can be written as:

$$\begin{aligned}\mathrm{H}^{\mathrm{HH}} = &\underbrace{-t\sum_{\langle ij\rangle}\left(\mathrm{a}^\dagger_i\mathrm{a}_j + H.c.\right) + U\sum_i \hat{\mathrm{n}}_{i\uparrow}\hat{\mathrm{n}}_{i\downarrow} + \sum_i v_i\hat{\mathrm{n}}_i}_{\mathrm{H}^e} \\ &+ \underbrace{\sum_i\left(\omega_0\mathrm{b}^\dagger_i\mathrm{b}_i + \sqrt{2}\eta\hat{\mathrm{x}}_i\right)}_{\mathrm{H}^{ph}=\mathrm{H}^{ph}_0+\mathrm{H}^{ph}_{ext}} + \underbrace{\sqrt{2}g\sum_i\hat{\mathrm{x}}_i(\hat{\mathrm{n}}_i-1)}_{\mathrm{H}^{e-ph}}\end{aligned} \tag{1}$$

Here $\hat{\mathrm{n}}_{i\sigma} = \mathrm{a}^\dagger_{i\sigma}\mathrm{a}_{i\sigma}$ is the fermionic number operator, and $\hat{\mathrm{x}}_i = (\mathrm{b}^\dagger_i + \mathrm{b}_i)/\sqrt{2}$ is the phononic displacement operator with the units chosen to that $\hbar = \omega_0 m = 1$, m being the nuclear mass. Wherever the spin-subscript is missing, a sum over spins has already been performed, so that $\mathrm{a}^\dagger_i\mathrm{a}_j = \sum_\sigma \mathrm{a}^\dagger_{i\sigma}\mathrm{a}_{j\sigma}$, and $\hat{\mathrm{n}}_i = \hat{\mathrm{n}}_{i\uparrow} + \hat{\mathrm{n}}_{i\downarrow}$. The system is chosen to be spin-compensated, so that $\langle\hat{\mathrm{n}}_{i\uparrow}\rangle = n_{i\uparrow} = n_{i\downarrow} = n_i/2$.

We start by examining the first part of the expression above, H^e, which is known as the Hubbard Hamiltonian. It was considered by Hubbard and others in 1963 as a way of describing narrow band transition metals which were not well described by other model systems used at the time [13, 14, 8]. The first term of the Hubbard-Hamiltonian describes the hopping of electrons between sites, where t is the magnitude of this hopping, $\langle ij\rangle$ denotes nearest neighbours and H.c. stands for hermitian conjugate. The electrons can thus only hop directly between nearest neighbour sites. This term accounts in the simplest way possible for the kinetic energy of the model. The magnitude of t describes the overlap between the basis states, and thus the model will approach the atomic limit as t decreases. The middle term in H^e is the Hubbard term, which accounts for an on-site interaction of strength U between electrons. This is a repulsive term which can describe the strong correlation effects found in some types of materials. The third term in H^e accounts for any on-site or external potential.

The second part, $\mathrm{H}^{ph} = \mathrm{H}^{ph}_0 + \mathrm{H}^{ph}_{ext}$, is a purely phononic Hamiltonian where the phonons are modelled as harmonic oscillators with frequency ω_0 and an external potential η. This potential is merely used as a tool to facilitate the analytical calculations.

The last term, H^{ph-e} is the Holstein-term which describes the interaction between electrons and phonons of strength g. It was introduced in 1959 by T. Holstein for the purpose of studying polarons [11]. This term will act attractively on the electrons, as shown in the following section.

1.1.1 The Lang-Firsov Transformation

The Lang-Firsov (LF) transformation is a unitary transformation which diagonalizes the phononic parts of the Hamiltonian H^{HH} and moves the effects of the electron-phonon coupling into the electronic part H^e by a rescaling of the hopping parameter t. It is useful for this thesis as it allows for some simplifications of the analytical calculations, by replacing the coupling term H^{e-ph} and the external phononic potential H^{ph}_{ext} in the phononic part of H^{HH} by a shift. The procedure amounts to a spatial translation of the phonon coordinates.

The transformed Hamiltonian $\tilde{\mathrm{H}}$ is given by:

$$\tilde{\mathrm{H}} = e^{i\mathrm{S}}\mathrm{H}e^{-i\mathrm{S}} \tag{2}$$

where S is defined as:

$$\mathrm{S} = -\frac{\sqrt{2}}{\omega_0}\sum_i \hat{\mathrm{p}}_i(g[\hat{\mathrm{n}}_i - 1] + \eta) \tag{3}$$

Here $\sqrt{2}\hat{\mathrm{p}}_i = i(\mathrm{b}^\dagger_i - \mathrm{b}_i)$ is the phonon momentum operator at site i.

The translational operator translating the spatial coordinate by a distance a looks like: $\mathrm{T} = e^{-i\hat{\mathrm{p}}a}$, and by analogy the LF-transformation thus corresponds to a "translation" $a = \hat{\mathrm{a}} = \sqrt{2}(g[\hat{\mathrm{n}}_i - 1] + \eta)/\omega_0$. The transformed Hamiltonian $\tilde{\mathrm{H}}$ looks explicitly like:

$$\tilde{\mathrm{H}} = \underbrace{\sum_i \left[\tilde{v}\hat{\mathrm{n}}_i + \tilde{U}\hat{\mathrm{n}}_{i\uparrow}\hat{\mathrm{n}}_{i\downarrow}\right] - \sum_{\langle ij\rangle}\left(\tilde{t}_{ij}\mathrm{a}_i^\dagger \mathrm{a}_j + h.c\right)}_{\tilde{\mathrm{H}}^e} + \underbrace{\sum_i \omega_0 \tilde{\mathrm{b}}_i^\dagger \tilde{\mathrm{b}}_i}_{\tilde{\mathrm{H}}_0^{ph}} - \frac{(\eta - g)^2}{\omega_0} \tag{4}$$

which looks like a Hubbard Hamiltonian ($\tilde{\mathrm{H}}^e$) with rescaled parameters plus a diagonal bosonic Hamiltonian ($\tilde{\mathrm{H}}_0^{ph}$), with the introduction of a shift $-(\eta - g)^2/\omega_0$ as anticipated. The electrons and phonons are now coupled via the rescaled electronic hopping parameter $\tilde{t}_{ij}$ instead of the coupling term. The rescaled parameters $\tilde{v}$, $\tilde{U}$ and $\tilde{t}_{ij}$ are defined according to:

$$\begin{aligned} \tilde{U} &= U - \frac{2g^2}{\omega_0} \\ \tilde{v} &= v + \frac{g^2}{\omega_0} - \frac{2g\eta}{\omega_0} \\ \tilde{t}_{ij} &= te^{i\sqrt{2}g(\hat{\mathrm{p}}_i - \hat{\mathrm{p}}_j)/\omega_0} \end{aligned} \tag{5}$$

In obtaining the expressions above it is important to not forget that $\hat{\mathrm{n}}_i = \hat{\mathrm{n}}_{\uparrow i} + \hat{\mathrm{n}}_{\downarrow i}$ and $\hat{\mathrm{n}}_{i,\sigma}^2 = \hat{\mathrm{n}}_{i,\sigma}$, as we are still dealing with operators and not expectation values. It is also noted that the rescaled hopping parameter $\tilde{t}_{ij}$ is now an operator and not a number.

For a system without the kinetic term of the electrons, such as the single site in contact with a bath examined in section 2.3, the Lang-Firsov transformation is more explicit in first quantization. Starting from the non-transformed purely phononic Hamiltonian, H^{ph}, we have:

$$\frac{\omega_0}{2}(\hat{\mathrm{p}}^2 + \hat{\mathrm{x}}^2) + \sqrt{2}\eta_0\hat{\mathrm{x}} = \frac{\omega_0}{2}\left(\hat{\mathrm{p}}^2 + (\hat{\mathrm{x}} + x_0)^2\right) - \frac{\eta_0^2}{\omega_0} \tag{6}$$

where $x_0 = \sqrt{2}\eta_0/\omega_0$ is the equilibrium position of the harmonic oscillator.

1.2 A short introduction to DFT

DFT is an in principle exact method for treating ground states of many-body systems. It reformulates quantum mechanics into a density-dependent theory which allows for a remapping of an interacting many-body system into non-interacting system with the same density. This greatly reduces the computational effort required to solve the many-body system, which is the key feature of

DFT as compared to other methods. The remapping of the interacting to a non-interacting system is what poses the primary challenge in DFT, as it requires the so called exchange-correlation potential (xc-potential), which is a highly complicated object. The aim of this thesis has been to investigate the xc-potential for the HH-model. The reason to study the xc-potential for this rather simple model is that for practical applications of DFT the xc-potential of a reference system is used to approximate that of the actual system of interest, as the exact xc-potential is in general not available. Therefore it is informative to study the HH-model and compare it to the Hubbard model to gain qualitative understanding of the role phonons play in the properties of the xc-potential as well as in the behaviour of materials with strong correlation effects.

1.2.1 Ground State Formalism

The basic procedure within DFT is outlined in two different papers written in the 60's [10, 16]. In the first paper Hohenberg and Kohn show how quantum mechanics can be reformulated to depend on the particle charge density n of a system, rather than the wavefunction. This is done by expressing the full ground state energy of the system as a functional of the density n, $E_0[n(\mathbf{r})] = E_0[n]$, which means that the total energy E_0 depends on the full density distribution $n(\mathbf{r})$ at all points in space. It is then shown how there is a one-to-one mapping between the ground state particle density n and the ground state energy E_0. This is referred to as the Hohenberg-Kohn (HK) theorem. Other proofs of this theorem have also been developed, among them one presented by Schönhammer et al [23], which is an extension to the constrained search method by Levy [19]. This approach is more general than the original proof and allows for reformulation in other densities than just the particle density, such as the current density. The constrained search method is used in section 2.1 to verify the legitimacy of using DFT in the particular case of the HH-model.

In the second paper, Kohn and Sham demonstrate how the theorem of Hohenberg and Kohn could be used to formulate a method for treating a many-body system of interacting particles via a non-interacting system of the same density, referred to as the Kohn-Sham (KS) system. This treatment can be argued for by the following: For the fully interacting system the total energy can be divided into different contributions. The total kinetic energy T can be separated into the contribution from a non-interacting system of the same density, T_0, and the contribution which comes from interactions between the particles, T_{xc}, so that $T = T_0 + T_{xc}$. The rest of the energy can be divided into the contribution from the external potential, E_{ext}, the Hartree energy E_H, which is obtained with the Hartree approximation (see 1.2.3) and the reminder ϵ_{xc}, which comes from interactions not considered at the Hartree level. Thus the total energy can be written as:

$$E_0[n] = T_0[n] + E_{ext}[n] + E_H[n] + E_{xc}[n] \tag{7}$$

where $E_{xc} = T_{xc} + \epsilon_{xc}$. All the contributions are functionals of the density n. As

$E_0[n]$ is a ground state energy, the variational principle gives that:

$$\begin{aligned} 0 = \delta E_0 &= \int dn \left(\frac{\delta T_0[n]}{\delta n} + \frac{\delta E_{ext}[n]}{\delta n} + \frac{\delta E_H[n]}{\delta n} + \frac{\delta E_{xc}[n]}{\delta n} \right) \\ &= \int dn \left(\frac{\delta T_0[n]}{\delta n} + v_{ext}[n] + v_H[n] + v_{xc}[n] \right) \end{aligned} \tag{8}$$

where $v_{xc}[n]$ thus contains the contributions from both T_{xc} and ϵ_{xc}.

Then we consider the corresponding KS-system, described by the many-body wavefunction $|\Psi_{\text{KS}}\rangle$, which by definition is non-interacting and has the same density as the fully interacting ground state. As the particles in the KS-system are non-interacting, $|\Psi_{\text{KS}}\rangle$ can be written as a Slater determinant of the single particle wavefunctions $|\phi_\lambda\rangle$, resulting in a set of equations looking like:

$$\left(\mathrm{T} + v_{\text{KS}}[n]\hat{\mathrm{n}}\right) |\phi_\lambda\rangle = \varepsilon_\lambda |\phi_\lambda\rangle \tag{9}$$

where T is the kinetic energy operator. The KS-potential v_{KS} must be chosen such that the density of the KS-system equals the density of the fully interacting system. The HK-theorem guarantees that there is no more than one such potential. A suitable choice for the KS-potential is, from equation (8):

$$v_{\text{KS}} = v_{ext} + v_H + v_{xc} \tag{10}$$

so that the KS-system will indeed have the same density as the interacting system. Expressed like this, all the physics beyond the Hartree level is contained in the xc-potential.

The density of the KS-system is given by

$$n(\mathbf{r}) = \sum_\lambda \left|\phi_\lambda(\mathbf{r})\right|^2 \tag{11}$$

where λ runs over all occupied states and a sum over spins has already been performed. Once the density is found, any observable can in principle also be determined from the one-to-one correspondence between the density and the full many-body wavefunction of the interacting system. There are however several problems arising along the way. As mentioned above, the HK-theorem guarantees that there is no more than one potential for the KS-system which reproduces the correct density. It does not, however, guarantee the existence of such a potential, which is referred to as the problem of $v-$representability [19]. Even if there exists an xc-potential corresponding to the system of interest, it is far from trivial to actually find this potential. Often the Local Density Approximation (LDA) is employed to simplify this task, in which the xc-potential is assumed local, i.e. it is considered a function of the local density instead of a density functional. Mathematically this is expressed as:

$$v_{xc}[n(\mathbf{r})] \xrightarrow{\text{LDA}} v_{xc}(n(\mathbf{r})) \tag{12}$$

Even so, there is no method for constructing the xc-potential for an arbitrary system, and thus for practical calculations the xc-potential of a reference system, such as the interacting free-electron gas or the Hubbard model, is used as an approximation of the actual xc-potential. It is thus clear within where the primary limitations of the DFT-method lies. Then to increase the versatility of DFT, the xc-potential of more intricate reference systems needs to be extracted, which is the essential aim of this thesis.

1.2.2 Time-Dependent (TD)DFT

The DFT-formalism can also be extended to time dependent systems, as initially shown by Runge and Gross in 1983 [21]. To construct the framework for TDDFT-calculations, we start in a similar way as for the time-independent case, by setting up the equations for the time-dependent Kohn-Sham system:

$$\big(\mathrm{T} + v_{\mathrm{KS}}(t)\big)\,|\phi_\lambda(t)\rangle = i\frac{\partial}{\partial t}\,|\phi_\lambda(t)\rangle \tag{13}$$

and similarly to before we get the density as

$$n(\mathbf{r},t) = \sum_\lambda \big|\phi_\lambda(\mathbf{r},t)\big|^2 \tag{14}$$

where the density now carries a time argument t in addition to the spatial argument $\mathbf{r}$. Equation (14) is, like for the ground state-formulation, by definition equal to the density of the fully interacting system.

The time dependence of the KS-Hamiltonian in equation (13) comes from the time dependence of the KS-potential, which can be divided into the external, Hartree- and xc-potentials as in equation (10). The time dependence of the external potential is trivial, and for the model studied in this project the Hartree potential is a function (and not a functional) of the density meaning that all intricate time dependence of the system, such as memory effects, needs to be accounted for by the xc-potential.

Thus the exact time-dependent xc-potential is an object which depends on the density not only at all points in space, as in the ground-state formulation, but also at all points in time. Therefore it is common practice to, in addition to the LDA, also assume that the density-dependence of v_{xc} is local in time, or adiabatic. This approximation is true in the limit where v_{KS} changes infinitely slow. This approximation is called the Adiabatic Local Density Approximation (ALDA) and has been used in this project for all time dependent DFT-calculations.

1.2.3 The Hartree and Hartree-Fock approximations for the HH-model

The Hartree approximation is one of the first approximation schemes developed for many-body systems. The basic assumption is that the many-body wavefunction can simply be written as a product state of single particle wavefunctions, and the ground state is defined as the product state with the lowest energy.

One of the greatest shortcomings of this method is that it doesn't recognize the antisymmetry of the electronic wavefunction, and it therefore misses both exchange and correlation effects. In practice it is not used much because of this, as much of the physics is lost with the lack of these contributions. However, it still accounts for a considerable contribution to the total energy, and thus to the KS-potential. Therefore it is considered within DFT in order to isolate the part of the KS-potential which contains the exchange and correlation effects.

The Hartree-Fock (HF) method is another many-body approximation scheme where the basic assumption is instead that the many-body wavefunction can be constructed as a Slater determinant of single particle orbitals, which is the simplest way to construct a many-particle solution that satisfies the antisymmetry of the fermionic wavefunction. The variational principle is used to find the HF ground state wavefunction as the Slater determinant with the lowest energy. The HF-method has been widely used, and is the first approximation method which recognizes the antisymmetry of the fermionic wavefunction, therefore accounting for the so called exchange-effects from fermion-fermion interactions.

The HH-Hamiltonian in equation (1) considers only one orbital per site and has a spin-explicit form of the Hubbard term. For this way of formulating the HH-Hamiltonian it can be shown that the contribution from considering the full Hartree-Fock scheme instead of only the Hartree scheme is zero. Therefore the potential v_H, which usually in DFT refers to the Hartree potential coming from cosidering the Hartree approximation, will throughout the rest of this thesis be referred to as the Hartree-Fock potential instead. This we do in order to make explicit how there is no Fock-contribution in the xc-potential of the HH-model in this project.

The HF-energy, E_H, and HF-potentials, v_H and η_H, for the HH-model are:

$$\begin{aligned} E_H(n,x) &= \sum_i U\frac{n_i^2}{4} + \sqrt{2}g\sum_i (n_i-1)x_i \\ v_H(n,x) &= \sum_i U\frac{n_i}{2} + \sqrt{2}g\sum_i x_i \\ \eta_H(n,x) &= g\sum_i (n_i-1) \end{aligned} \tag{15}$$

where v_H enters the electronic and η_H the bosonic KS-Hamiltonian respectively. The KS-equations for the HH-model are derived in section 2.1.

1.3 The Green's functions formalism and Dynamical Mean Field Theory (DMFT)

Dynamical Mean Field Theory (DMFT) is a non-perturbative method which finds an approximate single particle Green's function of a system through a self consistency scheme. The Green's function is a very powerful object through which much can be learned about the system it describes, such as the spectrum,

total energy and all single-particle expectation values. The single particle Green's function formalism is for example used when studying the behaviour of single charges moving in a field in electrodynamic problems. Also when studying a many-body system it is for many purposes sufficient to find the single particle Green's function, which then describes the propagation of a particle in a field given by all the other particles. Compared to DFT, DMFT has the advantage of not being in need of complicated a priori input, such as the xc-potential, but the disadvantage of being computationally much more taxing.

DMFT has been used in this project to find the total energy of the HH-model for an infinitely coordinated Bethe lattice. This lattice is characterized by not having any closed loops, and the coordination refers to the number of nearest neighbours at each lattice site. This is thus a rather non-physical lattice model, but is used as it reduces the computational effort needed to find the Green's function, and it could still yield qualitatively interesting results. The Bethe lattice is discussed in more detail in section 1.3.5. Once the total energy is found, the xc energy can be separated from the rest and differentiated with respect to the electronic density, n, and phononic displacement, x, to find the xc-potentials v_{xc} and η_{xc} respectively. The DMFT method can thus be used to find an xc-potential. This potential is exact so far as the DMFT-scheme is exact, which is in the limit of infinite dimensions. The xc-potential then allows for investigation of more elaborate systems at a much lower computational cost using (TD)DFT and the (A)LDA approximation.

1.3.1 Zero-temperature Green's functions

As mentioned above, the Green's function is a very useful object, through which several interesting properties of a system can be obtained. In quantum mechanics, the most important object is the wave function, which is the solution to the Shrödinger equation:

$$\left[i\hbar\frac{\partial}{\partial t} - \mathrm{H}(\mathbf{r})\right]\psi(\mathbf{r},t) = 0 \tag{16}$$

The Schrödinger equation is a linear, partial differential equation which is first order in time, and thus this discussion is valid for any such differential equation. As the Hamiltonian H in the above equation is time independent, this formulation only considers the equilibrium state. For a treatment of a system out of equilibrium, a time dependent Hamiltonian has to be introduced. The mathematical Green's function corresponding to the single particle Schrödinger equation is defined as the object $g(z,z')$ which solves:

$$\left[i\hbar\frac{\partial}{\partial t} - \mathrm{H}(\mathbf{r})\right]g(z,z') = \delta(z-z') \tag{17}$$

where the operator H is a time-independent, linear, hermitian operator and $z = \mathbf{r},t$. As H is time-independent, the absolute time arguments of $g(z,z')$, t and t', are not important but only the difference between them, $\Delta t = t - t'$. The

Green's function $g(z, z')$ must also obey the same boundary conditions as the single particle wavefunction $\psi(z)$.

To briefly understand some of the analytical behaviour of the Green's function, we start by expressing $g(z, z') = g(\mathbf{r}, \mathbf{r}', \Delta t)$ via it's Fourier transform w.r.t Δt:

$$g(\mathbf{r}, \mathbf{r}', \Delta t) = \int \frac{d\omega}{2\pi} e^{-i\omega\Delta t} g(\mathbf{r}, \mathbf{r}', \omega) \tag{18}$$

By substituting (18) into (17) we get

$$\begin{aligned} \big(\hbar\omega - \mathrm{H}(\mathbf{r})\big)\, g(\mathbf{r}, \mathbf{r}', \omega) = \delta(\mathbf{r} - \mathbf{r}') \rightarrow \\ g(\mathbf{r}, \mathbf{r}', \omega) = \sum_n \frac{\phi_n(\mathbf{r})\phi_n^*(\mathbf{r}')}{\hbar\omega - E_n} \end{aligned} \tag{19}$$

where the last line has been obtained by expressing $\delta(\mathbf{r} - \mathbf{r}') = \langle \mathbf{r} | \mathbf{r}' \rangle$, inserting a completeness relation and letting $\mathrm{H}(\mathbf{r})$ act on the states $|\phi_n\rangle$ after solving for $g(\mathbf{r}, \mathbf{r}', \omega)$.

We can now see that $g(\mathbf{r}, \mathbf{r}', \omega)$ is analytic in the complex ω-plane, save for the simple poles on the real axis (as H is Hermitian) corresponding to the eigenvalues of H, E_n. It is from this clear that $g(\mathbf{r}, \mathbf{r}', \omega)$ contains information about the energy levels of the system described by the Hamiltonian H.

To regain the time-dependent Green's function from equation (18) a limiting procedure must be performed in order to evaluate the Fourier integral, as $g(\mathbf{r}, \mathbf{r}', \omega)$ is not analytic on the real axis otherwise.

$$\begin{aligned} g^{\pm}(\mathbf{r}, \mathbf{r}', \Delta t) &= \lim_{\eta \to 0} \int \frac{d\omega}{2\pi} e^{-i\omega\Delta t} \sum_n \frac{\phi_n(\mathbf{r})\phi_n^*(\mathbf{r}')}{\hbar\omega - E_n \pm i\eta} \\ &= \frac{\pm i\theta(\pm\Delta t)}{\hbar} \sum_n e^{-iE_n\Delta t/\hbar} \phi_n(\mathbf{r})\phi_n^*(\mathbf{r}') \end{aligned} \tag{20}$$

Here the integral form of the Heavyside function $\theta(t)$ has been used to reach the last line. It can be seen that depending on the sign of Δt we get different Green's functions, g^+ and g^-. These are referred to as the retarded and advanced Green's function, respectively.

The Green's function usually referred to within physics is a single particle Green's function which is defined as:

$$G(z, z') = -i \langle \psi_0 | \, \mathrm{T}[\hat{\psi}(z)\hat{\psi}^\dagger(z')] \, | \psi_0 \rangle \tag{21}$$

where $|\psi_0\rangle$ is the many-body Heisenberg ground state and $\hat{\psi}(z)$ is the Heisenberg field operator which destroys a particle (creates a hole) at z. For simplicity $\hbar$ has now been set to one, which will be true throughout the rest of the discussion. T is the time ordering operator which reflects the behaviour of the Heavyside function in equation (20):

$$\mathrm{T}[\hat{\psi}(z)\hat{\psi}^{\dagger}(z')] = \begin{cases} \hat{\psi}(\mathbf{r},t)\hat{\psi}^{\dagger}(\mathbf{r}',t') & t > t' \\ \pm\hat{\psi}^{\dagger}(\mathbf{r}',t')\hat{\psi}(\mathbf{r},t) & t' > t \end{cases} \tag{22}$$

where the plus sign corresponds to bosons and the minus sign to fermions. For a non-interacting system the expression in equation (21) reduces to $g^{+} + g^{-}$, which can be seen by expressing (21) in the so called Lehmann representation (see e.g [7]).

$G(z, z')$ in equation (21) is referred to as the time ordered Green's function. It describes the propagation of a particle at z added to the system at z' when $t > t'$, and the propagation of a hole when $t' > t$. As a result of this, Green's functions are also referred to as propagators. The spin component of the fields $\hat{\psi}$ and $\hat{\psi}^{\dagger}$ has been omitted for simplicity, as spin symmetry is assumed throughout this thesis. Technically the single particle Green's function does however carry two spin indices, meaning the equations above only consider one spin channel.

1.3.2 Temperature Green's functions

The program used to obtain the data for this thesis evaluated the Matsubara or temperature Green's function to obtain information about the system. Therefore this section will give a short review on this extension of the Green's function formalism.

The temperature Green's function is defined as the thermal average of the Green's functions corresponding to all basis states, where the Hamiltonian is that of the grand canonical ensemble:

$$\mathrm{K} = \mathrm{H} - \sum_{i} \mu\hat{\mathrm{n}}_i \tag{23}$$

Here μ is the chemical potential and $\hat{\mathrm{n}}$ is the number operator. This substitution is convenient as it allows the possibility to vary the number of particles in the system by varying μ. The grand partition function Z and the statistical operator $\hat{\rho}^{T}$ are written as

$$Z = \sum_{n} \langle\psi_n| e^{-\beta\mathrm{K}} |\psi_n\rangle = e^{-\beta\Omega} \tag{24}$$

$$\hat{\rho}^{T} = \frac{e^{-\beta\mathrm{K}}}{Z} = e^{\beta(\Omega-\mathrm{K})} \tag{25}$$

where $\beta = 1/k_B T$ is the inverse temperature and k_B is the Boltzman factor. A modified Heisenberg picture is then introduced according to

$$\hat{\psi}_K(\mathbf{r},\tau) = e^{\mathrm{K}\tau}\hat{\psi}(\mathbf{r})e^{-\mathrm{K}\tau} \tag{26}$$

$$\hat{\psi}^{\dagger}_K(\mathbf{r},\tau) = e^{\mathrm{K}\tau}\hat{\psi}^{\dagger}(\mathbf{r})e^{-\mathrm{K}\tau} \tag{27}$$

which for a purely imaginary $\tau = it$ is formally identical to the regular Heisenberg picture. The variable τ is referred to as the imaginary time, and consequently the modified operator $\hat{\psi}_K(\mathbf{r}, \tau)$ is sometimes called the imaginary time operator. This reformulation is convenient as the Green's function formalism from the previous section can then be used to treat systems not only at zero-temperature but also at finite temperature.

The temperature Green's function will then look like:

$$G^T(\mathbf{r}, \mathbf{r}', \tau, \tau') = \sum_n \langle \psi_n | \, \hat{\rho}^T \mathrm{T}[\hat{\psi}(\mathbf{r}, \tau)\hat{\psi}^\dagger(\mathbf{r}', \tau')] \, | \psi_n \rangle = Tr\{\hat{\rho}^T \mathrm{T}[\hat{\psi}(\mathbf{r}, \tau)\hat{\psi}^\dagger(\mathbf{r}', \tau')]\} \tag{28}$$

where the time ordering is with respect to the imaginary times τ and τ'.

In the imaginary time formulation, the Green's function is periodic within the interval $-\beta < \tau - \tau' < \beta$, which simplifies the evaluation of the Green's function. The Green's function can be shown to be odd for fermions and even for bosons within this interval. This allows the Green's function to be expanded in a Fourier series, with only even/odd frequencies for bosons/fermions [7].

The non-interacting Green's function, corresponding to a non-interacting particle (no self-interactions either), can be written more explicitly in the frequency domain as:

$$G_0^T(\omega_m) = \sum_j \frac{\phi_j^0(\mathbf{r})\phi_j^0(\mathbf{r}')^\dagger}{i\omega_m - (\epsilon_j^0 - \mu)} \tag{29}$$

where $\phi_j^0(\mathbf{r})$ are the eigenfunctions of the non-interacting grand canonical Hamiltonian $\mathrm{K}_0 = \mathrm{H}_0 - \sum_i \mu \hat{\mathrm{n}}_i$ with eigenvalues $\epsilon_j^0 - \mu$. The Matsubara frequencies ω_m are given as:

$$\omega_n = \begin{cases} \frac{(2n+1)\pi}{\beta} & \text{fermions} \\ \frac{2n\pi}{\beta} & \text{bosons} \end{cases} \tag{30}$$

The expression in equation (29) is obtained by evaluating equation (28) for either fermions or bosons explicitly, and utilising the (anti) periodicity of the Green's function to evaluate the Fourier integral. In arriving at equation (29) only the difference between the two imaginary time arguments $\Delta\tau = \tau - \tau'$ has been considered, which requires the Hamiltonian to be independent of τ and τ'. We note how equation (29) and (19) look very similar.

In the case of a translationally invariant system the basis states $\phi_j^0 \to \phi_k$ can be written as plane waves of momentum $\mathbf{k}$, which makes it easy to identify the momentum dependent Green's function $G_0^T(\mathbf{k}, \omega_m)$ as

$$G_0^T(\mathbf{k}, \omega_m) = \frac{1}{i\omega_m - (\epsilon_k - \mu)} \tag{31}$$

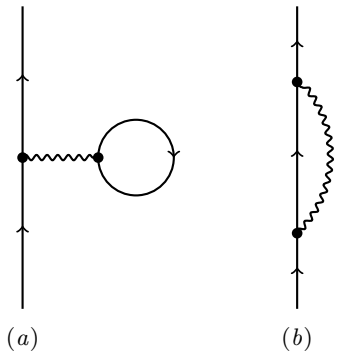

Figure 1: All first order Feynman diagrams for the propagation of a free particle.

1.3.3 Diagramatic expansion and Dyson's equation

The interacting Green's function, also called the dressed propagator, is evaluated through a perturbation expansion in terms of only the non-interacting Green's function and the inter-particle potential. To evaluate each term of the expansion is time consuming and cumbersome, and to simplify the task Wick's theorem is used (see e.g. [7]). This theorem provides a scheme for how to evaluate the terms in an easier way. The expansion can also be diagrammatically represented via Feynman diagrams, and through the Feynman rules the contribution to the interacting Green's function from any possible diagram can be evaluated in a straightforward way. The Feynman rules take their simplest form in momentum space, and therefore calculations are in general done in momentum space when possible.

In a Feynman diagram a propagating particle is usually represented by a solid line, and an interaction by a wavy line, where the former corresponds to G_0 and the latter to the interparticle interaction. The order of the diagram is given by the number of interaction lines. Figure 1 shows all first order diagrams for the propagation of a free particle.

For the second order there are ten different diagrams, displayed in figure 2. To get the full interacting Green's function G all Feynman diagrams of all orders need to be considered. This motivates defining the concept of a self-energy $\Sigma(z, z')$ and a proper self-energy $\Sigma^*(z, z')$ which are diagrammatically defined in figure 3. The self-energy is the sum of all possible Feynman diagrams with one ingoing and one outgoing particle line. The proper self-energy is defined in a similar way, but the Feynman diagrams making up the sum are only those which can not be reduced into lower-order diagrams by cutting a single particle line. All diagrams in figure 1 and 2 add to the self-energy, but only the diagrams in figure 1 and diagrams *e-j* in 2 add to the proper self-energy.

From the rhs in figure 3 we see that the interacting Green's function can be expressed recursively, if the non-interacting Green's function G_0 and the proper self-energy Σ^* are known:

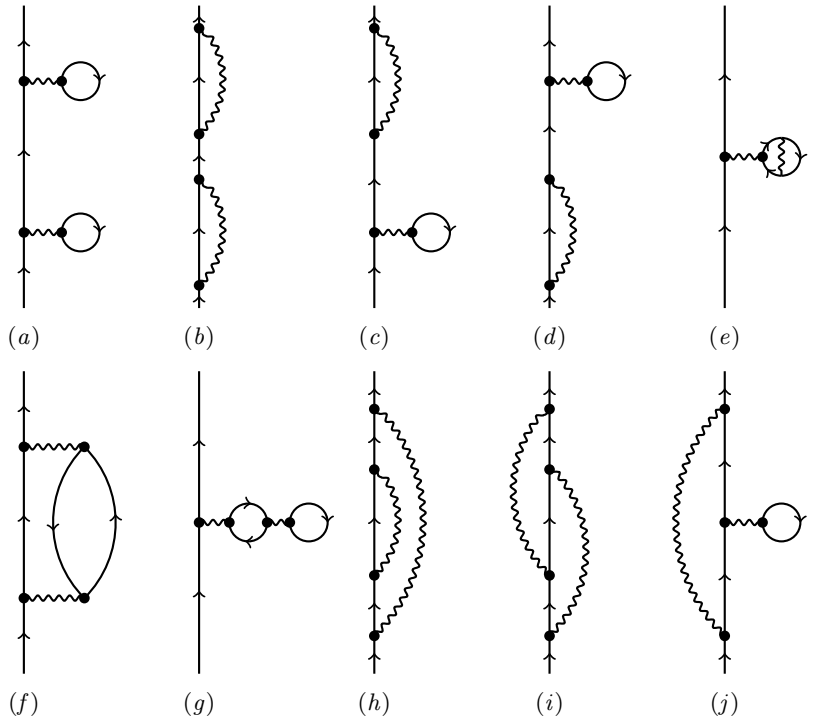

Figure 2: All second order Feynman diagrams for a free particle. Diagram a-d can be divided into the first order diagrams in figure 1 by cutting the propagator line. All diagrams add to the improper self-energy, while only (e-j) add to the proper self-energy.

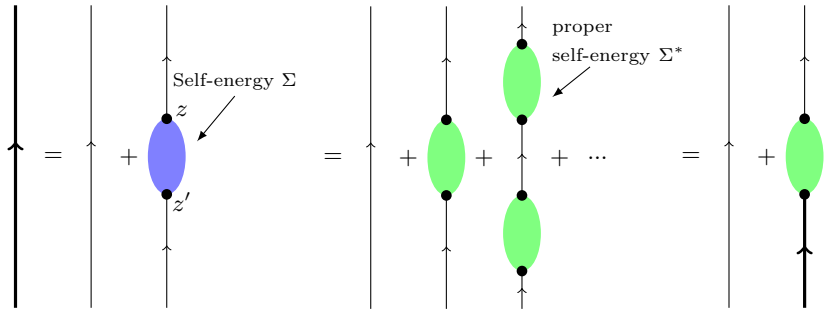

Figure 3: Diagrammatic definition of the self-energy Σ and proper self-energy Σ. The rhs is Dyson's equation expressed in a diagrammatic form.*

$$G(\mathbf{k},\omega_m) = G_0(\mathbf{k},\omega_m) + G_0(\mathbf{k},\omega_m)\Sigma^*(\mathbf{k},\omega_m)G(\mathbf{k},\omega_m) \tag{32}$$

This is referred to as Dyson's equation. Solving for G in equation (32) and inserting the expression for the non-interacting Green's function from equation (31) gives the expression for the interacting Green's function:

$$G(\mathbf{k},\omega_m) = \frac{1}{i\omega_m - (\epsilon_k^0 - \mu) - \Sigma^*(\mathbf{k},\omega_m)} \tag{33}$$

The local Green's function is defined as the spatial representation of the Green's function with identical spatial arguments: $G(\mathbf{r},\mathbf{r},\omega_m) = G_l(\mathbf{r},\omega_m)$. For a truly homogeneous and infinite system, the local Green's function $G_l(\mathbf{r},\omega_m)$ is thus independent of $\mathbf{r}$. We also define the density of states (DOS) as the quantity:

$$\rho(\mathbf{r},\epsilon) = \sum_k \delta(\epsilon - \epsilon_k)\phi_k(\mathbf{r})\phi_k^\dagger(\mathbf{r}) \tag{34}$$

and express the spatial representation of the local Green's function as

$$G_l(\mathbf{r},\omega_m) = \sum_k \frac{\phi_k^0(\mathbf{r})\phi_k^0(\mathbf{r})^\dagger}{i\omega_m - (\epsilon_k^0 - \mu) - \Sigma^*(\mathbf{k},\omega_m)} = \int d\epsilon \frac{\rho^0(\mathbf{r},\epsilon)}{x - \epsilon} \tag{35}$$

with $x = i\omega_m + \mu - \Sigma^*(\mathbf{k},\omega_m)$.

1.3.4 The DMFT procedure

DMFT is a non-perturbative method commonly employed to investigate strongly correlated systems. The method maps the problem of finding the many-body lattice Green's function into finding the many-body local Green's function of an impurity in contact with a bath. This impurity model is called the Anderson Impurity Model (AIM) and the mapping is in itself not an approximation. However, to do the mapping from a full lattice problem to the AIM the proper self-energy (referred to as only the self-energy in the following) needs to be momentum-independent, or local. The assumption of a local self-energy is true for systems of infinite dimensionality, but for any system of finite dimensionality it is an approximation. DMFT is thus exact for systems of infinite dimensions, but always an approximation for any physical system, with better accuracy expected for higher dimensionalities. As a matter of fact, DMFT performs well already in three dimensions.

The aim of DMFT is to find the local lattice Green's function, $G_l(\mathbf{r},\omega)$, by finding the Green's function of the Anderson impurity, $g(\omega)$. Under the assumption that the self-energy is momentum-independent and that the system is periodic, the local and impurity Green's functions, $G_l(\mathbf{r},\omega)$ and $g(\omega)$, are the same. The impurity Green's function is found through an iterative process and an eigenvalue problem solver. The solver can use different methods, such as exact diagonalisation (ED) or continuous time quantum Monte Carlo (CTQMC).

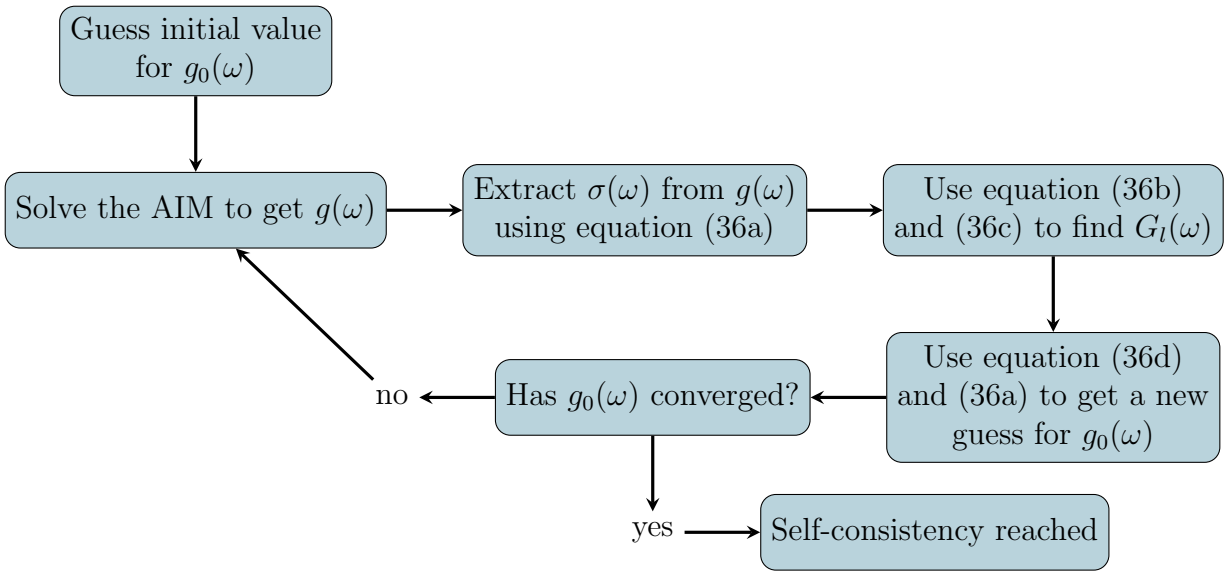

Figure 4: Flow chart describing the DMFT iterative process to find the local Green's function thorough an impurity model.

The iterative process is described schematically in figure 4 and below are some equations central to the procedure:

$$g(\omega) = [g_0(\omega)^{-1} - \sigma(\omega)]^{-1} \tag{36a}$$
$$\Sigma_l(\omega) = \sigma(\omega) \tag{36b}$$
$$G_l(\omega) = \sum_k [i\omega - \epsilon_k + \mu - \Sigma_l(\omega)]^{-1} \tag{36c}$$
$$g(\omega) = G_l(\omega) \tag{36d}$$

Here $\sigma(\omega)$ is the self energy of the impurity, and $g_0(\omega)$ is the non-interacting impurity Green's function given as

$$g_0(\omega) = \frac{1}{i\omega + \mu - \Delta(\omega)} \tag{37}$$

$\Delta(\omega)$ is called the hybridization function and is another kind of self energy, here describing the interaction between the impurity and the bath.

1.3.5 DMFT and the Bethe lattice

The Bethe lattice (or Cayley tree) is a lattice model commonly used to gain qualitative understanding of a certain Hamiltonian, as it has some properties which make it easier to do calculations on than e.g. on a cubic lattice. The Bethe lattice looks like an infinite tree where each lattice site is connected to a certain number of new sites given by the coordination number d. A schematic

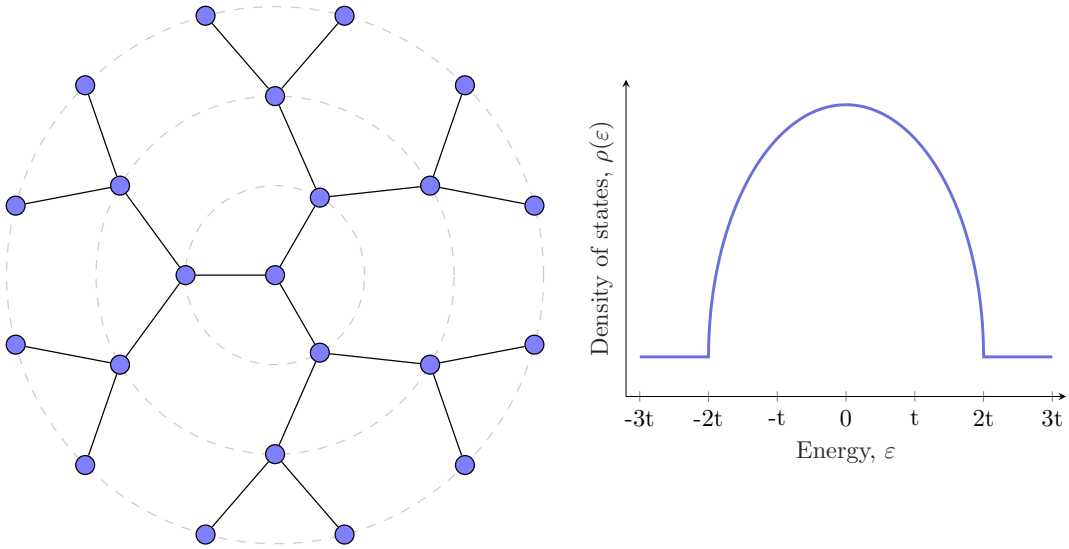

Figure 5: (left) Part of a Bethe lattice (Cayley tree) with coordination number $d = 3$. (right) Density of states for the infinitely coordinated Bethe lattice.

figure of a section of a Bethe lattice with coordination number $d = 3$ is shown to the left in figure 5. In contrast to a physical lattice it is impossible to visit one site twice without going backwards on a Bethe lattice, i.e. is has no closed loops. For the non-interacting, tight binding Bethe lattice in the limit $d \to \infty$ the density of states (DOS) takes an elliptical shape according to:

$$\rho(\epsilon) = \frac{1}{2\pi t^2}\sqrt{\epsilon^2 - 4t^2} \tag{38}$$

which has a fixed bandwidth of $4t$, where t is the hopping parameter. The DOS is shown schematically to the right in figure 5. The analytical form of the Bethe lattice DOS simplifies the DMFT-loop as some of the steps can be done analytically. Low dimensional lattices usually have a finite bandwidth, just as the infinitely coordinated Bethe lattice, but more complicated DOS, making the DMFT-loop more involved. Therefore the infinitely coordinated Bethe lattice is qualitatively useful as an approximation also for low dimensional lattices. Another benefit of the infinitely coordinated Bethe lattice is just that it is infinitely coordinated, and in this limit the DMFT-approximation $\Sigma(\mathbf{k}, \omega) \approx \Sigma(\omega)$ is not an approximation but an exact relation.

2 Theory

This section presents the analytical work that was done during this thesis project.

To establish the conceptual foundations for the applications of DFT to the HH-model, we prove the HK-theorem for the HH-model. This proof extends the derivation of reference [23], where a method for constructing the functional theory of an arbitrary set of observables $\{A\}$ is outlined, by first proving the HK-theorem and then deriving the KS-equations. The local charge density n_i was used as the observable describing the electrons, and the local displacement x_j was used for the phonons. These two quantities were chosen as they couple the two types of particles in the Hamiltonian from equation (1).

In order to extract the xc-energy E_{xc} from the information attained from the DFMT-code, the different contributions needed to be identified according to equation (7). This procedure is presented in section 2.2.

A simple realization was then carried out analytically for an HH-site in contact with a heat bath, where t was set to zero to simplify the problem. The Hartree-xc-potentials, $v_{Hxc} = v_H + v_{xc}$ and $\eta_{Hxc} = \eta_H + \eta_{xc}$ were found and investigated analytically and numerically. It was found that the results closely resemble those of a Hubbard site, as studied in [24, 26] and [22], but with rescaled parameters $\tilde{U}$ and $\tilde{v}$ given by equation (5) and the introduction of an additional term linear in $n-1$. The phononic xc-potential η_{xc} was found to be zero, although exchange-correlation effects are still present also for phonons through the coupling to the electrons.

2.1 Applicability of DFT to the Hubbard-Holstein model

The Hamiltonian for any system including electrons and phonons in the presence of local external fields can be written as:

$$\mathrm{H} = \mathrm{H}_0 + \sum_i v_i \hat{\mathrm{n}}_i + \sqrt{2} \sum_j \eta_j \hat{\mathrm{x}}_j \tag{39}$$

where v_i is the electronic external potential at site i and η_j is the phononic external potential at site j. H_0 is the rest of the Hamiltonian and can be chosen arbitrarily. The obvious choice for the purpose of this discussion is to choose the HH-Hamiltonian H^{HH} from equation (1) without the external terms as H_0.

$$\begin{aligned} \mathrm{H} = & \underbrace{-t \sum_{\langle ij \rangle} \mathrm{a}_i^\dagger \mathrm{a}_i + H.c + \omega_0 \sum_j \mathrm{b}_j^\dagger \mathrm{b}_j}_{\mathrm{H}_{ni}} \\ & + \sum_i U_i \hat{\mathrm{n}}_{\uparrow i} \hat{\mathrm{n}}_{\downarrow i} + g\sqrt{2} \sum_i \hat{\mathrm{x}}_i (\hat{\mathrm{n}}_i - 1) + \sum_i v_i \hat{\mathrm{n}}_i + \sqrt{2} \sum_j \eta_j \hat{\mathrm{x}}_j \end{aligned} \tag{40}$$

where H_{ni} has been defined, for later use, as the non-interacting part of the full Hubbard-Holstein Hamiltonian in equation (1).

The expectation values for the electronic density at site i and the phononic displacement at site j for a system described by the wavefunction $|\phi\rangle$ are denoted by

$$\langle\phi|\hat{\mathrm{n}}_i|\phi\rangle = n_i \quad , \quad \langle\phi|\hat{\mathrm{x}}_j|\phi\rangle = x_j \tag{41}$$

and to simplify the notation we write $\{n_i\} = n$ and $\{x_j\} = x$ in the following.

2.1.1 The HK-theorem

To prove the HK-theorem for the Hubbard-Holstein model we start by arguing that the total energy E can be written as a functional of the electronic charge density and the phonon displacement, $E[n, x]$, and then that this quantity must be minimized for the ground state density n^0 and displacement x^0. For this purpose we define a set $M[n, x]$ as the set of wavefunctions $|\phi[n, x]\rangle$ which results in the specific sets of eigenvalues n and x. Then we can define $F[n, x]$ as the minimum value in the set $\{\langle\phi|\,\mathrm{H}_0\,|\phi\rangle\}$, $|\phi\rangle \in M$, i.e.

$$F[n, x] = \min_{|\phi\rangle\in M} \langle\phi|\,\mathrm{H}_0\,|\phi\rangle \tag{42}$$

For a chosen state $|\Phi\rangle \in M$ for which H_0 attains it's minimal value $F[n, x]$, the total energy can be written as:

$$\begin{aligned} E[n, x] = \langle\Phi|\,\mathrm{H}\,|\Phi\rangle &= \langle\Phi|\,\mathrm{H}_0\,|\Phi\rangle + \langle\Phi|\sum_i v_i\hat{\mathrm{n}}_i + \sqrt{2}\sum_j \eta_j\hat{\mathrm{x}}_j\,|\Phi\rangle \\ &= F[n, x] + \sum_i v_i n_i + \sqrt{2}\sum_j \eta_j x_j \\ &\geq E_0 \end{aligned} \tag{43}$$

where E_0 is the ground state energy of H. This is a direct consequence of the variational principle, stating that the total energy of any state of the system described by the wavefunction $|\Phi\rangle$ is larger than or equal to the ground state energy of that system.

We then pick another wavefunction $|\Psi\rangle$ which is a ground state of H with the ground state energy E_0. We denote the expectation values of the electronic density and the phononic displacement for this system by:

$$\langle\Psi|\,\hat{\mathrm{n}}_i\,|\Psi\rangle = n_i^0 \quad , \quad \langle\Psi|\,\hat{\mathrm{x}}_j\,|\Psi\rangle = x_j^0 \tag{44}$$

The total energy of $|\Psi\rangle$ is then written as:

$$\begin{aligned} E_0 = \langle\Psi|\,\mathrm{H}\,|\Psi\rangle &= \langle\Psi|\,\mathrm{H}_0\,|\Psi\rangle + \langle\Psi|\sum_i v_i\hat{\mathrm{n}}_i + \sqrt{2}\sum_j \eta_j\hat{\mathrm{x}}_j\,|\Psi\rangle \\ &\geq F[n^0, x^0] + \sum_i v_i n_i^0 + \sqrt{2}\sum_j \eta_j x_j^0 \\ &= E[n^0, x^0] \end{aligned} \tag{45}$$

This follows from the fact that although $|\Psi\rangle \in M[n^0, x^0]$, it may not be a state for which $F[n^0, x^0]$ is attained. Hence we have obtained two inequalities from expression (43) and (45):

$$E[n, x] \geq E_0 \tag{46}$$
$$E[n^0, x^0] \leq E_0 \tag{47}$$

Expression (46) is true for every n and x, in particular for n^0 and x^0, and thus it must hold that

$$E[n, x] \geq E_0 = E[n^0, x^0] \tag{48}$$

With this we have shown that the total energy $E[n, x]$ is a functional of n and x which is minimized for the ground state density n^0 and displacement x^0. For a non-degenerate ground state n^0 and x^0 has been shown to have a one-to-one correspondence to the ground state energy $E_0[n^0, x^0]$, and they are completely determined by minimizing the total energy E. It is in this sense that DFT is a ground state theory.

2.1.2 The KS-system

We then need to verify the existence of the KS-equations, i.e. we need to find the set of single-particle equations which describe the non-interacting system with the same ground state density n and displacement x as the fully interacting ground state. The index indicating ground state expectation values from the previous section has been dropped, as the following discussion will only regard the ground state.

Since the total energy satisfies the variational principle w.r.t. n and x, the functional derivatives of E w.r.t n and x are zero in the ground state. This gives the two sets of Euler equations:

$$\frac{\delta F}{\delta n_i} + v_i = 0 \quad , \quad \frac{\delta F}{\delta x_j} + \sqrt{2}\eta_j = 0 \tag{49}$$

with $F[n, x]$ defined as in equation (42). To find the Kohn-Sham equations we decompose the total ground state energy $E[n, x]$ into different terms in such a way that the energy contribution from interactions within the system is isolated from the non-interacting contributions, similarly to equation (7).

$$E[n, x] = T^e_{ni}[n] + T^{ph}_{ni}[x] + E^e_{ext}[n] + E^{ph}_{ext}[x] + E^{ee}_H[n] + E^{e-ph}_H[n, x] + E_{xc}[n, x] \tag{50}$$

The two first terms are the kinetic energy for the electrons and phonons respectively for a non-interacting system of the same density n and displacement x as the ground state. We realize that these two terms give the energy $T^e_{ni} + T^{ph}_{ni} = E_{ni}$ which corresponds to H_{ni} in equation (40). The E^e_{ext} and E^{ph}_{ext} are the energies

originating from the external potential applied to the electrons and phonons respectively, followed by the HF-energies E_H^{ee} and E_H^{e-ph} for the electron-electron and electron-phonon interaction respectively. The last term is the xc-energy, containing everything left out by the other terms.

Taking the variation of the total energy yields:

$$\begin{aligned}
0 = \delta E &= \sum_i \frac{\delta E[n,x]}{\delta n_i}\delta n_i + \sum_j \frac{\delta E[n,x]}{\delta x_j}\delta x_j \\
&= \sum_i \delta n_i \left(\frac{\delta T^e_{ni}[n]}{\delta n_i} + \frac{\delta E^e_{ext}[n]}{\delta n_i} + \frac{\delta E^{ee}_H[n]}{\delta n_i} + \frac{\delta E^{e-ph}_H[n,x]}{\delta n_i} + \frac{\delta E_{xc}[n,x]}{\delta n_i} \right) \\
&\qquad + \sum_j \delta x_j \left(\frac{\delta T^{ph}_{ni}[x]}{\delta x_j} + \frac{\delta E^{ph}_{ext}[x]}{\delta x_j} + \frac{\delta E^{e-ph}_H[n,x]}{\delta x_j} + \frac{\delta E_{xc}[n,x]}{\delta x_j} \right) \\
&= \sum_i \delta n_i \left(\frac{\delta T^e_{ni}[n]}{\delta n_i} + v_i[n] + v^{ee}_{H,i}[x] + v^{e-ph}_{H,i}[n] + v^{xc}_i[n,x] \right) \\
&\qquad + \sum_j \delta x_j \left(\frac{\delta T^{ph}_{ni}[x]}{\delta x_j} + \sqrt{2}\left(\eta_j[x] + \eta^{e-ph}_{H,j}[n] + \eta^{xc}_j[n,x] \right) \right)
\end{aligned} \tag{51}$$

where the notation v^{ee}_H, v^{e-ph}_H and η^{e-ph}_H has been introduced as the HF-potential for the electron-electron and the electron-phonon interactions, and v_{xc} and η_{xc} as the xc-potential for electrons and phonons respectively.

We then make the substitutions

$$v^{\text{KS}}_i[n,x] = v_i[n] + v^{ee}_{H,i}[x] + v^{e-ph}_{H,i}[n] + v^{xc}_i[n,x] \tag{52}$$

and

$$\eta^{\text{KS}}_j[n,x] = \eta_j[x] + \eta^{e-ph}_{H,j}[n] + \eta^{xc}_j[n,x] \tag{53}$$

and note how equation (51) must be true for each index i, j separately. Hence we have two sets of coupled Euler equations:

$$\frac{\delta T^e_{ni}[n]}{\delta n_i} + v^{\text{KS}}_i[n,x] = 0 \quad , \quad \frac{\delta T^{ph}_{ni}[x]}{\delta x_j} + \sqrt{2}\eta^{\text{KS}}_j[n,x] = 0 \tag{54}$$

By comparison of equation (49) and (54) we realize that the latter must correspond to a system with the Hamiltonian

$$\text{H}^{\text{KS}} = \text{H}_{ni} + \sum_i v^{\text{KS}}_i \hat{\text{n}}_i + \sqrt{2}\sum_j \eta^{\text{KS}}_j \hat{\text{x}}_j \tag{55}$$

where we know H_{ni} from equation (1) and (40) to have no term which mixes the electrons and phonons. Thus $\text{H}_{ni} = \text{H}^e_{ni} + \text{H}^{ph}_{ni}$ describes a non-interacting system, and we can write down the Shrödinger-like KS-equations according to:

$$\left[-t\sum_{\langle ij\rangle}\left(\mathrm{a}_i^\dagger \mathrm{a}_j + \mathrm{a}_j^\dagger \mathrm{a}_i\right) + \sum_i v_i^{\mathrm{KS}} \hat{\mathrm{n}}_i\right] |\psi_\lambda^{\mathrm{KS}}\rangle = \varepsilon_\lambda^e |\psi_\lambda^{\mathrm{KS}}\rangle \tag{56}$$

$$\left[\omega_j \mathrm{b}_j^\dagger \mathrm{b}_j + \sqrt{2}\eta_j^{\mathrm{KS}} \hat{\mathrm{x}}_j\right] |\chi_{\lambda,j}^{\mathrm{KS}}\rangle = \varepsilon_{\lambda,j}^{ph} |\chi_{\lambda,j}^{\mathrm{KS}}\rangle \tag{57}$$

These equations are coupled through the KS-potentials v_{KS} and η_{KS}, and they describe the auxiliary KS-system, which is made out of non-interacting particles. Notice how the phononic part carries a site index j, meaning there is one equation for each site with a non-zero phonon interaction. The KS-system has the same electronic charge density n and phonon displacement x as the fully interacting system. In arriving at this we have made the assumption that the KS-potentials in equation (52) and (53) can be constructed. This is referred to as the v-representability condition, which is briefly discussed in section 1.2.1.

With this we have proved that the ground state energy E_0 is (for a non-degenerate ground state) fully determined by the ground state density n and displacement x, and vice versa, and that if this density and displacement can be recreated by any external potentials, these potentials are v^{KS} and η^{KS}.

2.2 Extracting the xc-energy

As has been mentioned earlier, a DMFT-code was used to construct the xc-potential of the HH-model for a small set of parameters. However, this code did not in fact provide neither the full potential nor the total energy, but some other various expectation values from which all different contributions to the total energy in equation (50) could be constructed. In this section we describe how the different energy terms are obtained, and thus how the xc-energy can be separated from the other contributions.

To find the xc-potentials we differentiate numerically the xc-energy w.r.t the electronic density n to get v_{xc} and w.r.t. the phononic displacement x to get η_{xc}.

The Hamiltonian used in the program is, as discussed in section 1.1.1, given by equation (1) and (4). No on-site energy was included, but an external chemical potential $-\mu$ acted on the system to adjust the density n. For fixed values of the electron-electron coupling U, electron-phonon coupling g, electron hopping t and phonon frequency ω_0 the external potentials μ and η were the only adjustable quantities, and thus they determine the density and the displacement. The phononic potential η contributes in a rather simple way as seen in equation (4) by rescaling the parameters and introducing a shift. The phononic potential η is therefore not considered by the code but handled analytically. The rescaled parameters are given by equation (5) as:

$$\begin{aligned}\tilde{U} &= U - \frac{2g^2}{\omega_0} \\ \tilde{\mu} &= \mu - \frac{g^2}{\omega_0} + \frac{2g\eta}{\omega_0} \\ \tilde{t}_{ij} &= te^{i\sqrt{2}g(\hat{\mathrm{p}}_i - \hat{\mathrm{p}}_j)/\omega_0}\end{aligned} \tag{5}$$

where the external potential v from section 1.1.1 has been set to be the chemical potential $-\mu$.

However, what we really want is the energy as a function not of μ and η but of n and x. The different expectation values needed to get the total energy for the system can be obtained with the DMFT-code, given a specific μ. By running the program for several different values of μ the different terms are obtained as functions of μ, as is the electronic density, $n(\mu)$. By inverting $n(\mu) \to \mu(n)$ the energy can be found as a function of n instead of μ. Thus it is clear that the value of μ is only important to get the corresponding density.

To also get rid of the phononic potential η we use the Heisenberg equation of motion:

$$\begin{aligned}0 = \frac{d\hat{\mathrm{p}}}{dt} = i[\hat{\mathrm{H}}, \hat{\mathrm{p}}] = -\omega_0 \hat{\mathrm{x}} - \sqrt{2}[g(\hat{\mathrm{n}} - 1) + \eta] \to \\ x = -\sqrt{2}[g(n-1) + \eta]/\omega_0\end{aligned} \tag{58}$$

where the average has been taken when going to the second line. From this the phononic potential η can be written in terms of x and n:

$$\eta(n, x) = -\frac{x\omega_0}{\sqrt{2}} - g(n-1) \tag{59}$$

The kinetic energy $\tilde{T}$ as given by the DFMT-program includes both interacting and non-interacting contributions. To extract the xc-energy these contributions need to be separated, which is done by numerically evaluating the kinetic energy T_0 for the non-interacting system, using an analytical closed form. The xc-kinetic-energy is then expressed as:

$$T_{xc} = \left\langle -\sum_{\langle ij \rangle} (\tilde{t}_{ij} \mathrm{c}_i^\dagger \mathrm{c}_j + H.c) \right\rangle - T_0 = \tilde{T} - T_0 \tag{60}$$

The non-interacting kinetic energy T_0 is obtained as a function of the chemical potential μ via the integral:

$$\begin{aligned}T_0(\mu) &= 2\int_{-\infty}^{\infty} \epsilon \rho(\epsilon) f(\epsilon, \mu, \beta) d\epsilon = \left[-\frac{1}{3\pi t^2}(4t^2 - \epsilon^2)^{3/2} \right]_{-2t, \beta=\infty}^{\mu} \\ &= -\frac{1}{3\pi t^2}(4t^2 - \mu^2)^{3/2}\end{aligned} \tag{61}$$

where $f(\epsilon, \mu, \beta)$ is the Fermi-distribution function which at zero temperature is a Heavyside function around μ, and the non-interacting DOS $\rho(\epsilon)$ for the Bethe lattice is given in equation (38). The DOS $\rho(\epsilon)$ is non-zero between $-2t$ and $2t$, where t is the hopping parameter. The factor 2 in front of the integral is there to account for both spin channels.

The density can be achieved in a similar way with the integral:

$$\begin{aligned} n(\mu) =& 2\int_{-\infty}^{\infty} \rho(\epsilon) f(\epsilon, \mu, \beta) d\epsilon \\ =& \frac{1}{\pi t^2}\left[\frac{\epsilon}{2}\sqrt{4t^2-\epsilon^2} + 2t^2 \tan^{-1}\left(\frac{\epsilon}{\sqrt{4t^2-\epsilon^2}}\right)\right]_{-2t,\beta=\infty}^{\mu} \\ =& \frac{1}{\pi t^2}\left(\frac{\mu}{2}\sqrt{4t^2-\mu^2} + 2t^2 \tan^{-1}\left(\frac{\mu}{\sqrt{4t^2-\mu^2}}\right)\right) + \frac{1}{2} \end{aligned} \tag{62}$$

where again the factor two is to include both spins.

There is no simple way to get an analytical expression for $T_0(n)$, as it would require us to solve for μ in equation (62). However, T_0 can still be obtained numerically for any density by evaluating the two equations above for the same μ.

We then note that the non-interacting phononic energy will explicitly look like:

$$E_0^{ph} = \omega_0 \langle \mathrm{b}^\dagger \mathrm{b} \rangle = \omega_0 \langle \tilde{\mathrm{b}}^\dagger \tilde{\mathrm{b}} \rangle - \frac{\eta_0^2}{\omega_0} - \sqrt{2}\eta_0 x \tag{63}$$

where η_0 is the external potential which results in the same displacement x for the non-interacting system as η would give in the interacting system. The potential η_0 is obtained from equation (59) by setting $g = 0$. As the ground state $|\tilde{\psi}_{ph}\rangle$ of the transformed phononic Hamiltonian is considered, $\langle \tilde{\mathrm{b}}^\dagger \tilde{\mathrm{b}} \rangle = 0$. This state must be considered to get the correct phononic displacement x, which can be understood from equation (6) in the discussion of the Lang-Firsov transformation in section 1.1.1. The same result is achieved from simple reasoning around the rhs of equation (63): the two first terms can be seen as a transformed phononic Hamiltonian with an external potential η_0, from which the contribution of the external potential is subtracted with the last term.

We can now write an expression E_{tot} for the total energy of the system where the contributions from the external potentials μ and η have been subtracted. We can also express all contributions to E_{tot} in terms of attainable expectation values, save for the xc-energy. The total energy and all contributions are expressed below. In rewriting the expressions onto a form independent of μ and η equation (5) and (59) has been used.

$$
\begin{aligned}
E_{tot} &= \tilde{U}\,\langle \mathrm{n}_\uparrow \mathrm{n}_\downarrow \rangle + \tilde{T} + \omega_0 \langle \tilde{\mathrm{b}}^\dagger \tilde{\mathrm{b}} \rangle \overbrace{-(\tilde{\mu}-\mu)n - (\eta - g)^2/\omega_0 - \sqrt{2}\eta x}^{=\frac{x^2\omega_0}{2} + \frac{g^2 n}{\omega_0}(n-1) + \sqrt{2}gx(n-1)} \\
E_0^e &= T_0 \\
E_0^{ph} &= -\eta_0^2/\omega_0 - \sqrt{2}\eta_0 x = \frac{x^2\omega_0}{2} \\
E_H^{e-e} &= Un^2/4 \\
E_H^{e-ph} &= \sqrt{2}gx(n-1)
\end{aligned}
\tag{64}
$$

Now the result above can be inserted into the full expression for the xc-energy:

$$
\begin{aligned}
E_{xc} &= E_{tot} - T_0 - E_0^{ph} - E_H^{e-e} - E_H^{e-ph} \\
&= \tilde{U}\,\langle \mathrm{n}_\uparrow \mathrm{n}_\downarrow \rangle + \tilde{T} + \omega_0 n_{ph} + \frac{x^2\omega_0}{2} + \frac{g^2 n}{\omega_0}(n-1) + \sqrt{2}gx(n-1) \\
&\quad - T_0 - \frac{x^2\omega_0}{2} \\
&\quad - U\frac{n^2}{4} - \sqrt{2}gx(n-1) \\
&= \tilde{U}\,\langle \mathrm{n}_\uparrow \mathrm{n}_\downarrow \rangle + \tilde{T} - T_0 + \omega_0 n_{ph} + \frac{g^2 n}{\omega_0}(n-1) - U\frac{n^2}{4}
\end{aligned}
\tag{65}
$$

2.3 Application of DFT to a single HH-site

In this section we derive the exact xc-potentials for a simple system of one HH-site in contact with a heat bath of inverse temperature β, with the hopping parameter t set to zero. This derivation extends the results of [22, 24] and the follow-up work of [26], where a similar calculation is performed for the pure Hubbard model. The thermal averages of n and x are found via the grand canonical partition function as functions of the potentials v and η. The results are inverted to find the expressions for the potentials as functions of n and x. The expressions (52) and (53) are then used to find an expression for the Hartree-xc- and xc-potentials v_H, v_{xc}, η_H and η_{xc}. Some of the more involved steps of this derivation are not presented explicitly in this section, but can be found in appendix A.

We write the local grand canonical Hamiltonian H_s of the single site system in second quantization as:

$$
\mathrm{K}_s = v_s \hat{\mathrm{n}} - \mu \hat{\mathrm{n}} + U \hat{\mathrm{n}}_\uparrow \hat{\mathrm{n}}_\downarrow + \omega_0 \mathrm{b}^\dagger \mathrm{b} + \sqrt{2} g \hat{\mathrm{x}}(\hat{\mathrm{n}} - 1) + \sqrt{2}\eta \hat{\mathrm{x}} \tag{66}
$$

which differs from the HH-Hamiltonian in equation (1) by the lack of the kinetic term describing the hopping between sites. The removal of the kinetic term simplifies the problem in such a way it can be solved analytically. We define the electronic potential v to account for both the chemical potential μ which

couples the site to the bath, and any other external or on-site potential v_s so that $v = v_s - \mu$.

The expectation values n and x can be found through differentiation of the partition function:

$$n = -\frac{1}{\beta}\frac{\partial \ln(\mathrm{Z})}{\partial v} \qquad \text{and} \qquad x = -\frac{1}{\beta\sqrt{2}}\frac{\partial \ln(\mathrm{Z})}{\partial \eta} \tag{67}$$

Therefore, we start by evaluating the partition function $\mathrm{Z} = \mathrm{Tr}\left(e^{-\beta \mathrm{K}_s}\right)$. The electronic part of this expression is easy to evaluate. There are four possible electronic configurations at the site: $|0\rangle$, $|\uparrow\rangle$, $|\downarrow\rangle$ and $|\uparrow\downarrow\rangle$, which all have a definite eigenvalue w.r.t the density operator: $n = 0, 1, 1, 2$. Using the phononic number states as basis for the phononic part, any state of the full basis to the Hamiltonian in equation (66) can be written as $|im\rangle$ where i denotes the electronic and m the phononic part. However, the phononic number states $|m\rangle$ are not eigenstates of the displacement operator $\hat{\mathrm{x}}$, and so we use the Lang-Firsov transformation described in section 1.1.1 to make the phononic part diagonal in the phononic occupation number basis. For simplicity we also make the substitution $\eta - g \to \zeta$. The transformed Hamiltonian will look like:

$$\tilde{\mathrm{K}}_s = \tilde{v}\hat{\mathrm{n}} + \tilde{U}\hat{\mathrm{n}}_\uparrow\hat{\mathrm{n}}_\downarrow + \omega_0 \mathrm{b}^\dagger \mathrm{b} - \frac{\zeta^2}{\omega_0} \tag{68}$$

where we have from equation (5):

$$\tilde{U} = U - \frac{2g^2}{\omega_0}$$
$$\tilde{v} = v + \frac{g^2}{\omega_0} - \frac{2g\eta}{\omega_0} = v - \frac{g^2}{\omega_0} - \frac{2g\zeta}{\omega_0}$$

Thus we get an expression for the partition function as:

$$Z = \sum_i \sum_{m=0}^{\infty} \langle im|\, e^{-\beta(\tilde{v}\hat{\mathrm{n}} + \tilde{U}\hat{\mathrm{n}}_\uparrow\hat{\mathrm{n}}_\downarrow + \omega_0 \mathrm{b}^\dagger \mathrm{b} - \zeta^2/\omega_0)}\, |im\rangle \tag{69a}$$

$$= \sum_{m=0}^{\infty} e^{-\beta(\omega_0 m - \zeta^2/\omega_0)} \left(1 + 2e^{-\beta\tilde{v}} + e^{-\beta(\tilde{U}+2\tilde{v})}\right) \tag{69b}$$

$$= \frac{e^{\beta\zeta^2/\omega_0}}{1 - e^{-\beta\omega_0}} \left(1 + 2e^{-\beta\tilde{v}} + e^{-\beta(\tilde{U}+2\tilde{v})}\right) \tag{69c}$$

where the first term in (69b) comes from the electronic state $|0\rangle$, for which $n = 0$. Similarly the second term comes from the states $|\uparrow\rangle\,/\,|\downarrow\rangle$ for which $n = 1$, and the last term from $|\uparrow\downarrow\rangle$ where $n = 2$. We finally get from (69b) to (69c) by recognising the geometrical sum $\sum_m^\infty e^{-\beta\omega_0 m} = (1 - e^{-\beta\omega_0})^{-1}$.

Now the partition function has been evaluated, and we can differentiate it w.r.t μ and η according to equations (67), in order to attain expressions for n and x. The expression for the density n will read:

$$n(\tilde{v}, \tilde{U}) = 2\frac{e^{-\beta\tilde{v}} + e^{-\beta(\tilde{U}+2\tilde{v})}}{1 + 2e^{-\beta\tilde{v}} + e^{-\beta(\tilde{U}+2\tilde{v})}} \tag{70}$$

Equation (70) can be compared to the expression given for the Hubbard site examined in [26], and we see that they are the same with the substitutions $\tilde{v} \to v$ and $\tilde{U} \to U$.

In expressing the displacement x we identify n after differentiating w.r.t. ζ and recognize that $\partial\zeta/\partial\eta = 1$.

$$x(\tilde{v}, \tilde{U}) = -\sqrt{2}\left(\frac{\zeta + gn(\tilde{v}, \tilde{U})}{\omega_0}\right) \tag{71}$$

By inverting the expression in (70) and making the substitution $n = 1 + \delta n$, $-1 > \delta n > 1$ we get the expression for $\tilde{v}(\delta n)$, from which we can solve for $v(\delta n, x)$:

$$\begin{aligned} v(\delta n, x) &= \tilde{v}(\delta n) + \frac{g^2}{\omega_0} + \frac{2g\zeta}{\omega_0} \\ &= -U + \frac{g^2}{\omega_0}(1 - 2\delta n) - \sqrt{2}gx \\ &\qquad - \frac{1}{\beta}\ln\left[\frac{\delta n + \sqrt{\delta n^2 + e^{-\beta\tilde{U}}(1 - \delta n^2)}}{1 - \delta n}\right] \end{aligned} \tag{72}$$

When the electron-phonon coupling g goes to zero, this expression reduces to that of the Hubbard model. To extract the xc-potential from equation (72) we solve for $v_{Hxc} = v_{xc} + v_H$ in equation (52). An expression for the KS-potential v_{KS} is attained by evaluating equation (72) for $U = g = 0$. This gives for v_{Hxc}:

$$\begin{aligned} v_{Hxc}(\delta n, x) &= v_{\text{KS}}(\delta n) - v(\delta n, x) \\ &= \left(U - \frac{2g^2}{\omega_0}\right) + \sqrt{2}gx + \frac{g^2}{\omega_0}(2\delta n + 1) \\ &\qquad + \frac{1}{\beta}\ln\left[\frac{\delta n + \sqrt{\delta n^2 + e^{-\beta\tilde{U}}(1 - \delta n^2)}}{1 + \delta n}\right] \end{aligned} \tag{73}$$

where the first parenthesis is $\tilde{U}$. This term replaces U in the expression for v_{Hxc} for a Hubbard site from [26] and can therefore be interpreted as a renormalized electron-electron interaction. From this we can see that the phonon coupling

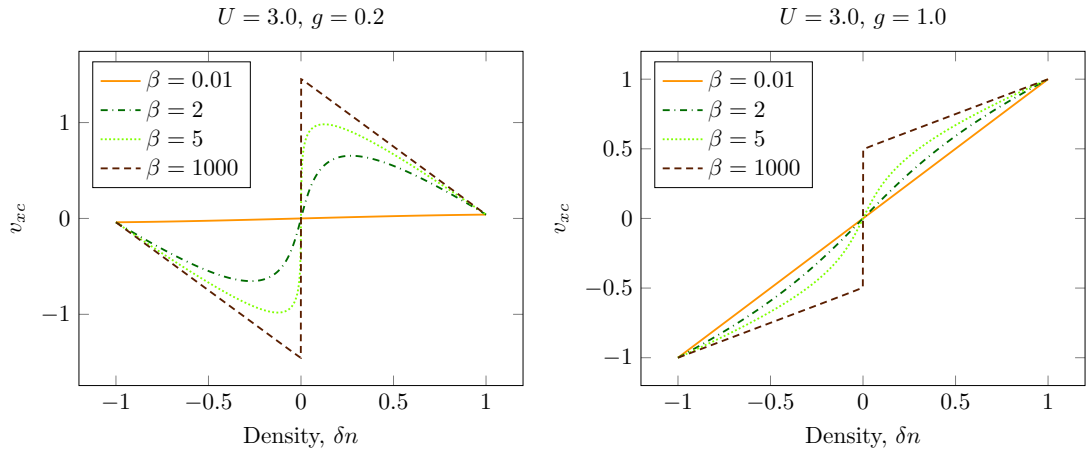

Figure 6: Xc-potentials for four different temperatures corresponding to $\beta = 0.01$, 2, 5, *and* 1000. *For both plots the electronic interaction is* $U = 3.0$, *and the electron-phonon interaction is* $g = 0.2$ *and* $g = 1.0$ *from left to right. The brown, dashed lines corresponding to* $\beta = 1000$ *show a tilted step function for both values of* g, *which is the expected behaviour in the limit* $\beta \to \infty$ *given by equation* (79). *For smaller values of* β *the function smoothens, shown by the green dotted-dashed and densely dotted lines. The orange, solid lines shows the behaviour expected for* $\beta = 0$ *in equation* (80).

will have an attractive effect on the electrons as the introduction of a (positive) non-zero g will decrease the effective on-site interaction $\tilde{U}$. The third term, $\sqrt{2}gx$, is the HF-term for the electron-phonon interaction. By subtraction of the HF-terms we get the xc-potential as:

$$v_{xc}(\delta n, x) = \frac{2g^2}{\omega_0}\delta n + \frac{\tilde{U}}{2} + \frac{1}{\beta}\ln\left[\frac{\delta n + \sqrt{\delta n^2 + e^{-\beta\tilde{U}}(1-\delta n^2)}}{1+\delta n}\right] - \frac{U}{2}\delta n \tag{74}$$

By following the same procedure for the phononic potential $\eta_{Hxc} = \zeta_{Hxc} - g$ as we did to find v_{Hxc}, we obtain the expression:

$$\eta_{Hxc}(n, x) = g(n-1) \tag{75}$$

which is only the phononic HF-term for the phonon-electron interaction. Thus, the phononic xc-potential is zero.

2.3.1 Analytical and numerical study of the xc-potential

In the following we look more closely at the peculiarities of the xc-potential in equation (74). The potential $v_{xc}(\delta n)$ is depicted for some different values of β and one set of values for U, g and ω in figure 6.

For the discussion, we start by identifying $f(\delta n)$ as:

$$f(\delta n) = \frac{\tilde{U}}{2} + \frac{1}{\beta} \ln \left[\frac{\delta n + \sqrt{\delta n^2 + e^{-\beta \tilde{U}}(1 - \delta n^2)}}{1 + \delta n} \right] \tag{76}$$

This is an odd function w.r.t δn, which may be easily verified by proving $f(-\delta n) = -f(\delta n)$ and simplifying the expression. We limit our discussion to the case $\tilde{U} > 0$ as this is true for the majority of our calculations. However, $\tilde{U} > 0$ has not been assumed during the derivation of v_{xc} and the result is valid for all values of $\tilde{U}$. The following discussion does however assume $\tilde{U} > 0$ and is not valid for negative values of $\tilde{U}$.

By identifying $f(\delta n)$ in equation (74) the v_{xc} can be simplified to:

$$v_{xc}(\delta n) = -\frac{U}{2}\delta n + \frac{2g^2 \delta n}{\omega_0} + f(\delta n) \tag{77}$$

where we can see that also the remaining terms of v_{xc} are odd in δn, and we note that $v_{xc}(\delta n = 0) = 0$. Thus all of v_{xc} is odd around half-filling. Expressing the v_{xc} in this way it is clear how any non-trivial behaviour comes from the $f(\delta n)$-term, which is where we will concentrate our efforts for this section.

We will start by studying $f(\delta n)$ in the zero-temperature limit, $T \to 0$, or equivalently $\beta \to \infty$. In this limit $f(\delta n)$ becomes a step-function, something that can be seen numerically. The magnitude of the gap is found by evaluating $f(\delta n = \pm 1)$. We find $f(\delta n = -1)$ by making a Taylor expansion in $e^{-\beta \tilde{U}}(1 - \delta n^2)$ around zero, which is a small number in the limit $\beta \to \infty$.

$$\lim_{\beta \to \infty} f(\delta n = -1) = -\tilde{U}/2 \tag{78}$$

As we have already concluded, $f(\delta n)$ is odd, meaning that $f(\delta n = 1) = \tilde{U}/2$ and thus the magnitude of the gap is $\tilde{U}$.

In the limit $\beta \to \infty$ the potential v_{xc} will then have the shape of a tilted step function given by:

$$v_{xc} = \begin{cases} -\frac{\tilde{U}}{2} + \left(\frac{2g^2}{\omega_0} - \frac{U}{2} \right) \delta n & \delta n < 0 \\ \frac{\tilde{U}}{2} + \left(\frac{2g^2}{\omega_0} - \frac{U}{2} \right) \delta n & \delta n > 0 \end{cases} \tag{79}$$

which is seen by inserting $f(\delta n = -1)_{\beta \to \infty} = \tilde{U}$ into equation (77). We see that $v_{xc} \neq 0$ at the end points at $\delta n = \pm 1$ except in the cases $\tilde{U} = 0$ or $g = 0$. The limit $\beta \to \infty$ is shown by the brown, dashed lines in figure 6, where $\beta = 1000$.

For $\beta < \infty$ the function will smoothen, seen by the green dotted-dashed and densely dotted lines in figure 6, and for $\beta \to 0$ the potential will resemble a straight line given by

$$v_{xc}(\delta n)_{\beta \to 0} = \left(\frac{2g^2}{\omega_0} - \frac{U}{2} \right) \delta n + \frac{\tilde{U}}{2}\delta n = \frac{g^2}{\omega_0}\delta n \tag{80}$$

shown by the orange, solid lines in figure 6. The second contribution to the slope, $\tilde{U}/2$, comes from

$$\lim_{\beta \to 0} f(\delta n) = \frac{\tilde{U}}{2} \delta n \tag{81}$$

which is realized by making a Taylor expansion of $f(\delta n)$ in $\beta \tilde{U}$ around 0.

3 Numerical Simulations

Within this thesis, the Hxc-potentials, v_{Hxc} and η_{Hxc}, obtained in section 2.3, equations (73) and (75), have been used to study two different systems. These are shown in figure 7.

The system in figure 7a shows a dimer with one HH-site (blue) and one non-interacting site (green). At the HH-site the electrons experience a repulsive interaction of strength U and they also interact with the phonon mode represented by an harmonic oscillator. The non-interacting site is acting as the bath of section 2.3. Figure 7b shows a linear chain with four HH-sites in an external potential.

Both systems in figure 7 were studied in their ground state for a set of different parameters U, g and t. System 7a was also studied during time evolution with a perturbation due to a varying external potential v_{ext}. For both ground state and time evolution calculations, the (TD)DFT scheme and the LDA and ALDA-approximations described in section 1.2 were used. The systems have also been solved using exact diagonalisation (ED) [2] and the HF-treatment, in order to evaluate the performance of the Hxc-potentials.

The code performing the DFT- and HF-calculations for both systems and the ED-calculation for the system shown in figure 7a was developed during the course of the thesis. This section describes the computational methods used to perform these simulations. The results are presented in section 4.1 and 4.2.

The xc-potential was also extracted for a small set of coupling parameters, $U = 3.0, 8.0$, $g = 0.2, 1.0$, using a DMFT-code [1]. The code was used to find the Green's function of an AIM as described in section 1.3 and extract some different expectation values contributing to the total energy according to section 2.2. The xc-energy was then separated from the total energy using equation (65).

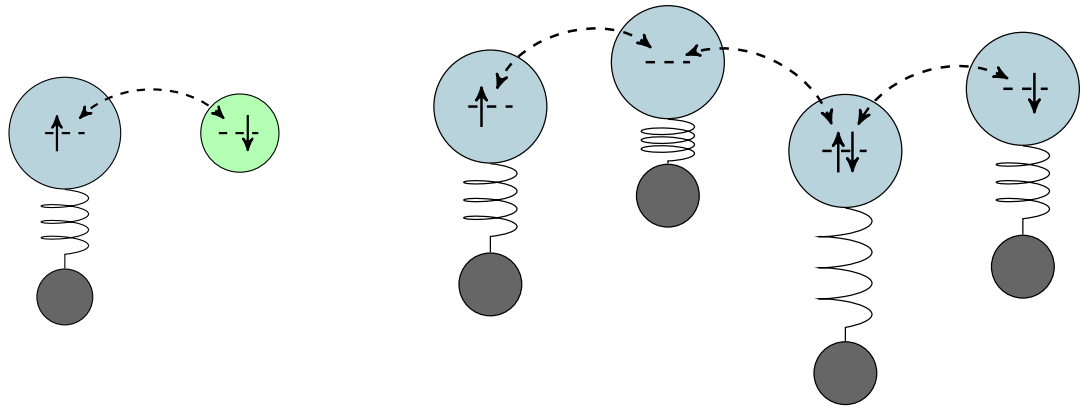

Figure 7: (a) Schematic figure of the dimer system studied in section 4.1 with interactions on one site (blue). (b) Schematic figure of the 4-site linear chain studied in section 4.2 with interactions on all sites.

3.1 Choosing a β

The potentials derived in section 2.3 and studied more closely in section 2.3.1 were used to study the behaviour of both systems in figure 7. In doing so, we notice that these potentials are derived for a model with a zero hopping parameter $t = 0$, and a finite temperature, while the models we study have a non-zero hopping parameter, and are in the ground state, corresponding to zero temperature. However, the merit in these potentials does not lie in their usefulness for practical applications, but in their ability to illustrate qualitative features of the xc-potential.

The quantum fluctuations not considered by setting $t = 0$ can arguably be compensated for by thermal fluctuations present at finite temperatures. Therefore the inverse temperature β was, for the purpose of these simulations, not set to infinity corresponding to zero temperature. Instead β was set to a finite value, imitating the effect of a non-zero hopping parameter t. As seen in figure 6, a finite β smoothens the potential and removes the discontinuity around half-filling. This is convenient for computational purposes, as the discontinuity can cause the DFT self consistency loop to oscillate around half-filling, preventing it to converge.

When simulating the dimer in figure 7a, β was optimized to give the best possible agreement between the exact and DFT-solutions for the initial state. The optimization procedure was done for each set of parameters U, g and t. The same value was used throughout the time evolution. The values attained in this way did, in general, correspond to rather heavily smoothened potentials. They were also dependent on the on-site potential, suggesting that adjusting β does not fully account for the approximations that has been made in the derivation of the xc-potentials, and the ALDA-approximations.

For the four-site chain in figure 7b, β was chosen based on the value found for similar values of the parameters U, g and t for the dimer.

3.2 Ground state calculations

To find the ground state of our HH-systems the Hamiltonian H from equation (1) or (55) is written in it's matrix form, with the matrix elements $\langle\phi_a|\,\mathrm{H}\,|\phi_b\rangle$. The basis states $\{\phi_i\}$ form a complete set of states spanning the space of H, although they are not in general eigenstates of H. This is straightforward for the fermionic part of the system, due to the Pauli exclusion principle assuring there is a finite number of states for a finite system. However, as the number of interacting fermions increase, the number of states increases very rapidly, so that large systems can in practice not be considered. This is the familiar problem of many-body physics.

Phonons do not obey the Pauli exclusion principle and the number of phonon states is therefore not limited to a finite number. This means that in principle an infinite number of basis states is needed to account for the phononic part of the system. However, in the ground state only the lowest energy states of the phonons will be populated and only a sufficient number of basis states needs

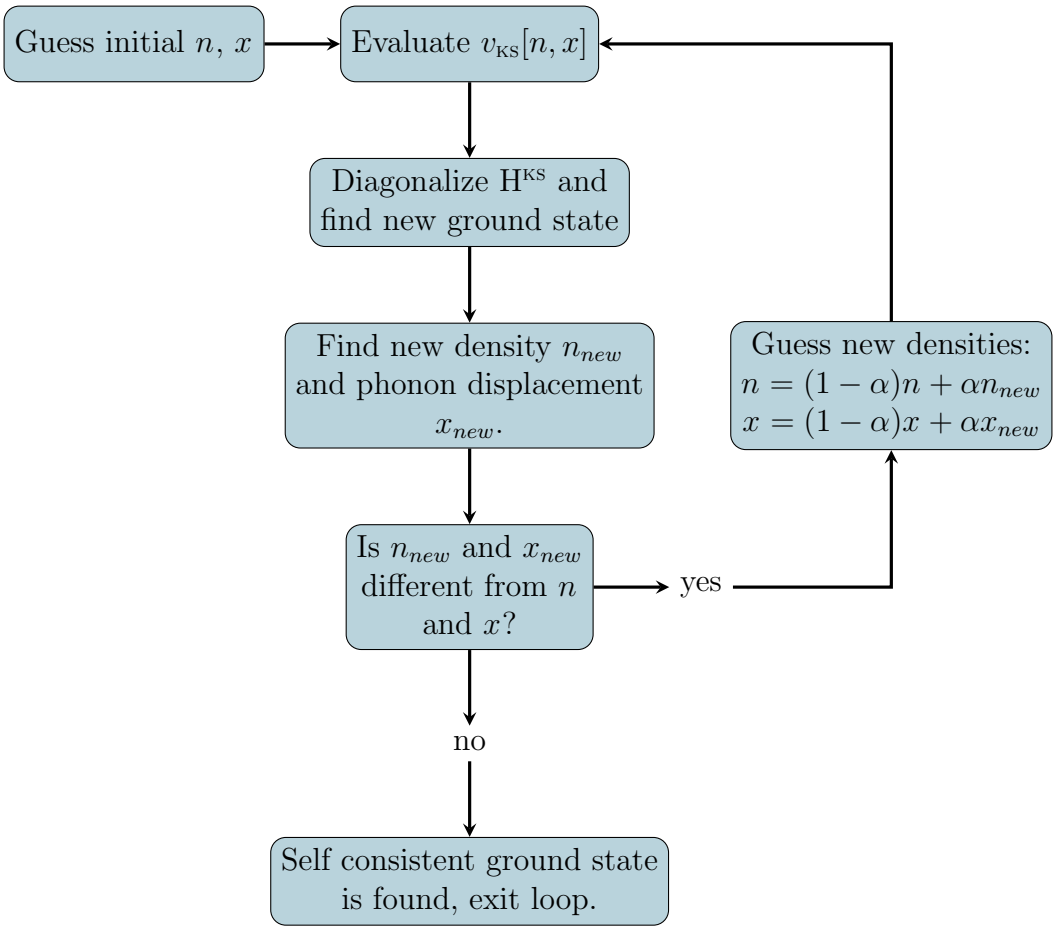

Figure 8: Self consistency procedure for obtaining the ground state of the KS-system.

to be considered. In order to realize whether a sufficient number of states has been considered or not, the simulations need to be run several times with an increasing number of states considered, until the results from successive runs are within some accepted tolerance.

The fermionic basis states used for the simulations were the local number states for each spin channel. The systems under considerations are closed systems at half filling, so that for a system of N sites there are $N/2$ spin-up and spin-down electrons respectively. To each site a phononic mode is also coupled, resulting in N harmonic oscillators of frequency ω_0, each to be described by a truncated subspace of M phonon number states.

3.2.1 Exact Diagonalization

In the exact diagonalisation (ED) method the full matrix Hamiltonian is diagonalized to solve the system. For the system of N sites with $N/2$ electrons in each spin channel and one phononic oscillator at each site described above, the number of fermionic states amounts to

$$N_f = \binom{N}{N/2}^2 \tag{82}$$

For each phonon mode added to the system, the number of fermionic states is multiplied with M, so that the total number of states for the HH-system is:

$$N_{tot} = N_f \times M^N \tag{83}$$

which grows very fast with N, although by restricting the total energy of the configurations considered, as only the lowermost states will be populated in the ground state, the problem can be reduced to some extent.

In all ED-calculations done in this thesis, a LAPACK-routine was used to do the diagonalisation.

3.2.2 HF- and DFT-approximation

The computational methods for the HF- and DFT-methods only differ from each other in the characteristics of the potential used to construct the auxiliary KS-system which approximates the interacting system. In the following we will refer to this external potential as v_{KS} regardless of approximation method, as the only difference is whether v_{KS} has a term v_{xc} or not.

As the particles are non-interacting (not coupled) in the KS-system, the many-particle problem is reformulated into many single-particle problems. As the system is spin compensated, only one of the spin channels needs to be considered, and for each spin channel there is now N fermionic states. Similarly the phonons are also considered separately, resulting in N separate problems with M states in each. Thus for the KS-system multiple smaller single particle Hamiltonians needs to be considered.

As the KS-potentials v_{KS} and η_{KS} depend on the density n and displacement x, which in turn depends on the KS-potentials, the KS-ground state is found through an iterative self consistency scheme, shown in figure 8. This iterative process requires the Hamiltonian to be diagonalized multiple times before the ground state is found, but as the size of the KS-Hamiltonian is so much smaller than the fully interacting one, the computational effort is still much smaller than that needed to solve the fully interacting system.

3.3 Time Evolution

The time dependence in this project was introduced via a time dependent external potential acting on the electrons. For the purpose of the simulations, time was discretised, so that the Hamiltonian was considered constant within each time step. For the exact solution, the Hamiltonian is known at each point in time, as there is only the explicit time dependence of the external potential to consider. Thus the propagation of the exact solution from time t to time $t + \Delta t$ would look like:

$$\begin{aligned} |\psi(t+\Delta t)\rangle &= e^{-i\mathrm{H}(t+\Delta t/2)\Delta t}\,|\psi(t)\rangle \\ &= \sum_{\lambda} e^{-iE_{\lambda}(t+\Delta t/2)\Delta t}\,|\lambda(t+\Delta t/2)\rangle\,\langle\lambda(t+\Delta t/2)|\psi(t)\rangle \end{aligned} \tag{84}$$

where Δt is the length of each time step and $|\lambda(t + \Delta t/2)\rangle$ are the eigenstates of the Hamiltonian H at time $t + \Delta t/2$.

For the DFT and HF-methods, however, there is in addition to the explicit time dependence of the perturbation an implicit time dependence in the v_{KS} through the xc-potential, which depends on the time-dependent quantities $n(t)$ and $x(t)$. To account for this a predictor-corrector scheme was used to approximate the KS-Hamiltonian in each time step. A predictor-corrector step is done as follows:

1. Evaluate the predictor Hamiltonian of time step $t+\Delta t = t_{n+1}$: $\mathrm{H}_p(\psi_{\text{KS}}(t_n), t_n) \equiv \mathrm{H}_p(t_n)$
2. Time propagate the KS-wavefunction $|\psi_{\text{KS}}\rangle$ from time t_n to t_{n+1} using $\mathrm{H}_p(t_n)$: $|\psi^p_{\text{KS}}(t_{n+1})\rangle = e^{-i\mathrm{H}_p(t_n)\Delta t}\,|\psi_{\text{KS}}(t_n)\rangle$
3. Find the corrector Hamiltonian $\mathrm{H}_c(\psi^p_{\text{KS}}(t_{n+1}), t_{n+1}) \equiv \mathrm{H}_c(t_{n+1})$
4. Use the average $\mathrm{H}_{\text{KS}}(t_n) = \frac{\mathrm{H}_p(t_n)+\mathrm{H}_c(t_{n-1})}{2}$ to propagate $|\psi_{\text{KS}}(t_n)\rangle$ to t_{n+1} using $\mathrm{H}_{\text{KS}}(t_n)$: $|\psi_{\text{KS}}(t_{n+1})\rangle = e^{-i\mathrm{H}_{\text{KS}}(t_n)\Delta t}\,|\psi_{\text{KS}}(t_n)\rangle$

This procedure will require the Hamiltonian to be diagonalized twice in each time step, instead of only once as for the ED-method, but the drastically smaller size of H_{KS} still makes this method much more computationally efficient.

3.4 DMFT-calculations

The details of the code used to perform the DMFT-calculations are not part of this project, but the general procedure of the DMFT-method is described in sections 1.3.4 and 1.3.5 [1]. The code performed the steps 2) to 5) on page 17, while the loop had to be closed and the convergence checked externally. The AIM-solver in step 2) used a CTQMC algorithm to find the impurity Green's function.

The x-dependence of the xc-energy was determined analytically according to section 2.2. The code took as input the interaction parameters U and g, the inverse temperature β and the chemical potential μ. In order to sample the total energy at different densities, the effective chemical potential μ had to be changed. The density and other expectation values, as discussed in section 2.2, could then be obtained through the program once the DMFT-loop had converged.

The DMFT-code evaluated the temperature Green's function discussed in section 1.3.2, although we wanted the zero temperature Green's function, meaning β should in principle be set to infinity. For the purpose of this project, β was set to 200.

4 Results and Discussion

In this section we present the results from the different simulations performed during the course of this project. Firstly we study the performance of the analytic v_{Hxc} and η_{Hxc} developed in section 2.3 for the two different systems described in section 3. The systems are shown schematically in figure 7. The results are compared to those obtained through exact diagonalisation (ED) and with the HF-potential.

Then, the xc-potential v_{xc} was constructed from the xc-energy E_{xc} of the infinitely coordinated Hubbard-Holstein Bethe lattice for a small but representative set of interaction parameters: $U = 3.0, 8.0$, $g = 0.2, 1.0$. The xc-energy was obtained through the procedure explained in section 2.2. Only ground states were considered in these calculations.

4.1 Ground State and Dynamics of a Dimer

The v_{Hxc} and η_{Hxc} from section 2.3 have here been used with the self-consistency scheme in figure 8 to study a dimer consisting of one HH- and one non-interacting site, as depicted in figure 7a. The results were compared to those of the ED- and HF-methods in the ground state and during time propagation of the dimer. Several different sets of the parameters U, g and t were used, while $\omega_0 = 1$ for all simulations. In the following a small subset of these simulations is presented, chosen as to reflect the general trends of the system. The external potentials used to perturb the system were a trigonometric and a Gaussian potential. The trigonometric potential was given as:

$$\begin{cases} \frac{A}{2}(1 - \cos(\frac{\pi t}{T_r})) & t \leq T_r \\ A & t > T_r \end{cases} \tag{85}$$

where A is the strength and T_r the length of the perturbation, referred to as the ramping time. The external potential acted on the non-interacting site by increasing the on-site energy. The density n and the phononic displacement x are shown for the exact and DFT-methods, while only the x-coordinate is shown for the HF-solution.

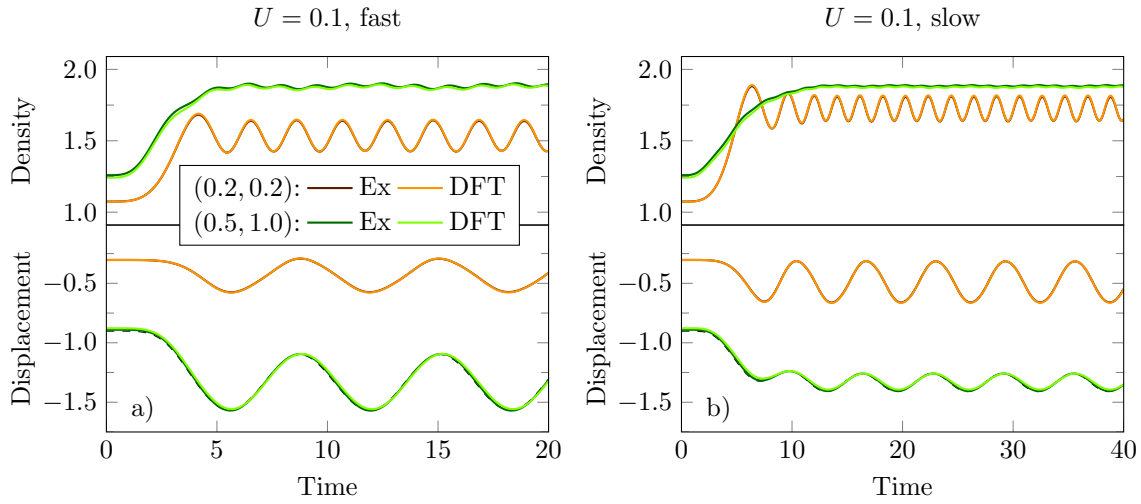

Figure 9: Electronic density and phonon displacement at the interacting site for two weakly coupled systems with $U = 0.1$. The solid light coloured lines correspond to the DFT solution and the darker to the exact. The black, dashed lines seen in the lower sections are the HF-solutions for the phonon coordinate. The different methods have for these systems given hardly distinguishable solutions. The orange lines corresponds to a system with $(g, t) = (0.2, 0.2)$ and the green to $(g, t) = (0.5, 1.0)$. Panel a) corresponds to a trigonometric perturbation increasing the on-site energy for the non-interacting site from 0 to 3 during 7 time units. In panel b) the ramping time of the perturbation is instead 14 time units. Note the different timescales of a) and b).

4.1.1 The weak coupling regime

First we study two weakly coupled systems in figure 9 with electronic coupling $U = 0.1$, and phonon-electron coupling g and hopping parameter t indicated as (g, t) in the figure legend. Two different trigonometric perturbations were used, which acted as an external electronic potential on the non-interacting site, going from 0 to 3 during 7 or 14 time units corresponding to panel a) and b) respectively.

We can see how the agreement between all three solutions is very good for these systems on both time scales. The agreement is best for the system represented by orange with parameters $(g, t) = (0.2, 0.2)$, even though the perturbations are not very adiabatic for this system, something that is indicated by the large amplitude of the oscillation and the fact that the average values of the observables is different between panel a) and b). This system has small values for both g and t and is the more weakly coupled of the two systems. That the agreement between all three solutions is so good, even though the perturbations are not very adiabatic, implies that the exchange and correlation effects are negligible for a system this weakly coupled.

Due to the larger values of the hopping parameter t, the response of the system represented by green with parameters $(g, t) = (0.5, 1.0)$ is more adiabatic in character. The oscillations in x are for the faster perturbation larger than for the orange system, which is due to the larger electron-phonon coupling g.

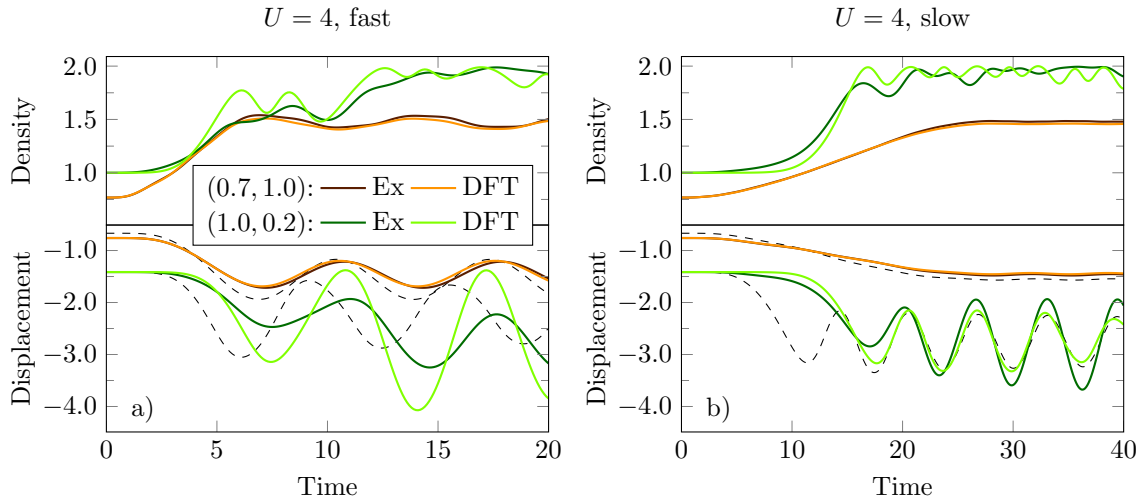

Figure 10: Electronic density and phonon displacement at the interacting site for two intermediately coupled systems with $U = 4$. The orange lines corresponds to a system with $(g, t) = (0.7, 1.0)$ and the green to $(g, t) = (1.0, 0.2)$. In panel a) the perturbation is the same as in figure 9a), and in panel b) the ramping time of the perturbation is instead 28 time units. Note the different timescales of a) and b).

4.1.2 The intermediate coupling regime

We then proceed to the intermediate coupling regime shown in figure 10 where the two systems have a much stronger electronic interaction of $U = 4$. The system represented by orange has parameters $(g, t) = (0.7, 1.0)$ and the one represented by green $(g, t) = (1.0, 0.2)$. The agreement for these systems is not as good as for the more weakly coupled systems in figure 9, but the DFT-solution can be seen to perform noticeably better than the HF-solution which is encouraging.

We can yet again see how the system with the smaller hopping parameter, the one represented by green, has a less adiabatic response to the perturbation than the one represented by orange, and also how the agreement between the DFT- and exact solution increases as the perturbation is made slower from panel a) to b).

It could be argued that the potentials from section 2.3 should perform better in the small t-limit, as they were developed for a system with $t = 0$. However, in the limit where $t \to 0$, that is when the overlap between the sites goes to zero, the electrons can't move between the two sites and the dynamics can therefore not be adiabatic. The poor agreement between the solutions for the system represented by green implies that for small values of t the ALDA introduced in section 1.2.2 is not a good approximation.

It can also be noted that the agreement is better for the system with smaller g, as was the case in figure 9.

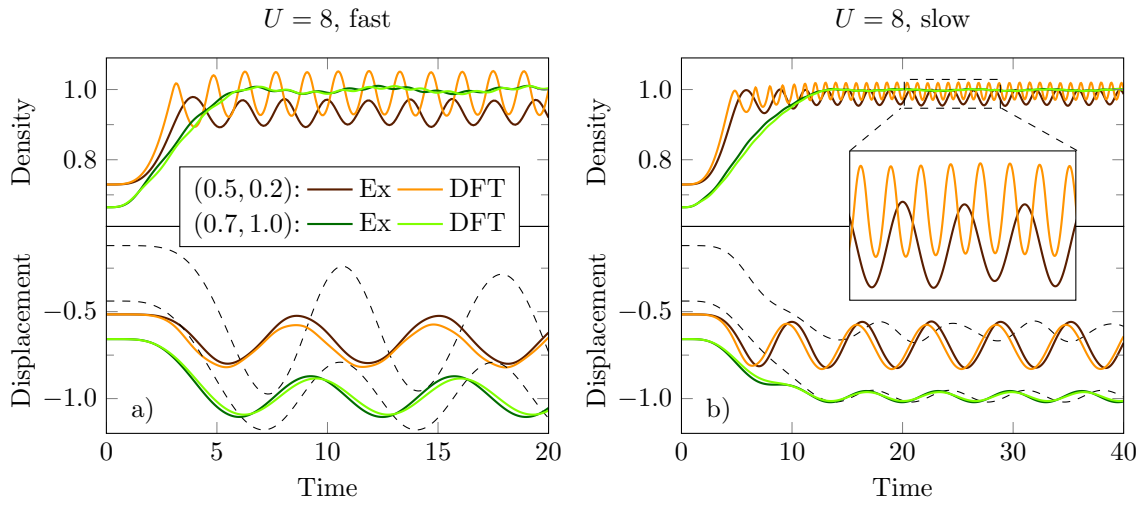

Figure 11: Electronic density and phonon displacement at the interacting site for two strongly coupled systems with $U = 8$. The orange lines corresponds to a system with $(g, t) = (0.5, 0.2)$ and the green to $(g, t) = (0.7, 1.0)$. The perturbations are the same as in figure 9 for both panels respectively. Note the different timescales of a) and b).

4.1.3 The strong coupling regime

Next to be studied is the strong coupling regime with figure 11 where $U = 8$. The system represented by orange has parameters $(g, t) = (0.5, 0.2)$ and the one represented by green has $(g, t) = (0.7, 1.0)$. Just as in the previous plots, the system with the smaller hopping parameter, i.e. the system represented by orange, is less adiabatic. It has also less good agreement between the ED- and DFT-solutions than the system represented by green, even though it has a smaller value for g. This further strengthens the conclusion that when t is small the ALDA is not a good approximation for these perturbations.

The agreement does not improve as obviously as in figure 10 for the slower perturbation. This could however be attributed to the fact that the time is only doubled between panel a) and b) in figure 11 as opposed to quadrupled in figure 10. The oscillations of the DFT-solution in this figure occur, as opposed to the previous cases, around half filling, which is where the discontinuity of v_{xc} is when $\beta \to \infty$. Even though v_{xc} used here has a value of β making it far from discontinuous, it still changes quickly around half filling, which could be the origin of the oscillations in the density [17]. The exact solution does not oscillate around half filling but slightly below, and looking at the HF-solution for the density (not shown) it does not show this rapidly oscillating behaviour at all.

For these systems we can also see how the HF-solution completely fails at predicting the initial ground state. It is overall evident how the HF-method overestimates the effective electron-electron repulsion at the interacting site for the strongly coupled systems. This leads to an underestimated displacement of the phononic coordinate, due to a too low electronic density at the interacting

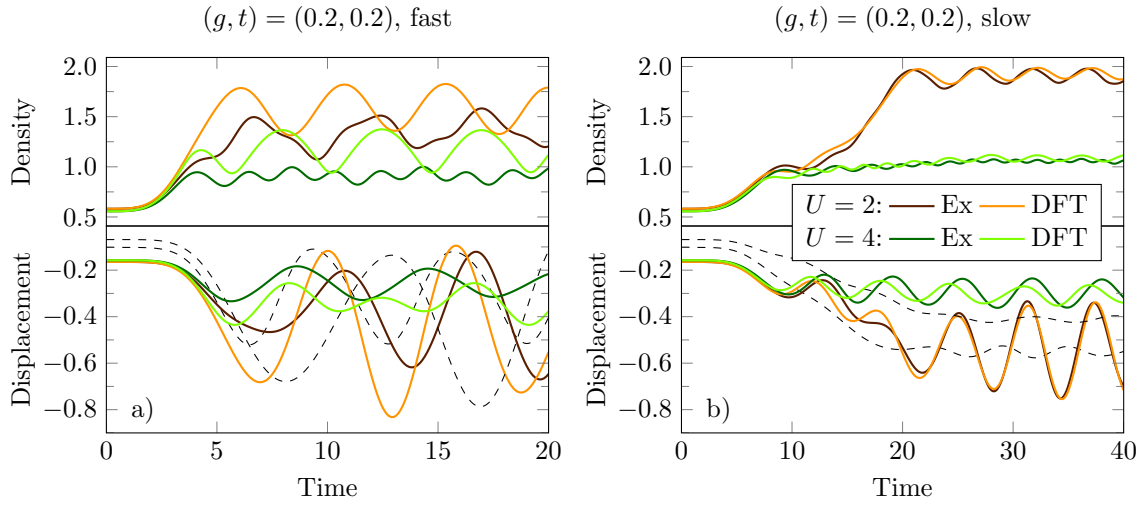

Figure 12: Electronic density and phonon displacement at the interacting site for two intermediately coupled systems with $t = 0.2$ and $g = 0.2$. The orange lines corresponds to a system with $U = 2$ and the green to $U = 4$. The perturbations are as in figure 10 for both panels respectively. Note the different timescales of a) and b).

site. From both figure 10 and 11 it can be seen that the HF-solution performs less poorly for smaller values of g in this regard.

4.1.4 The small-t-regime

Lastly for this perturbation we look at two systems in figure 12 with $g = 0.2$ and $t = 0.2$, but with different U. In panel a) the perturbation goes from 0 to 3 in 7 time units, as for all of the other left hand panels. We see how the agreement between the different solutions is very poor even though g is small. The HF-solution underestimates the phononic coordinate just as before, and more so for the larger U. Proceeding to panel b), where the perturbation lasts for 28 time units, the agreement has increased considerably, and DFT performs much better than the HF-solution here. From these sets of plots it is thus very clear that a small t requires a slow perturbation for the ALDA-approximation to yield useful results. We can also see that the agreement is best for the system represented by orange, corresponding to the more weakly coupled system with $U = 2$, which is unsurprising.

Just as for the strongly interacting systems in figure 11 the HF-solutions in figure 12 overestimates the effective electron-electron repulsion. In panel b) the HF-solution also lack most of the dynamic behaviour.

4.1.5 A Gaussian perturbation

In figure 13 another type of perturbation has been used, namely a Gaussian with a full width half maximum (FWHM) of 7 time units and an amplitude of 3 in panel a), and FWHM of 14 and an amplitude of 1.5 in panel b). It is centred around $t = 14$ and $t = 28$ respectively.

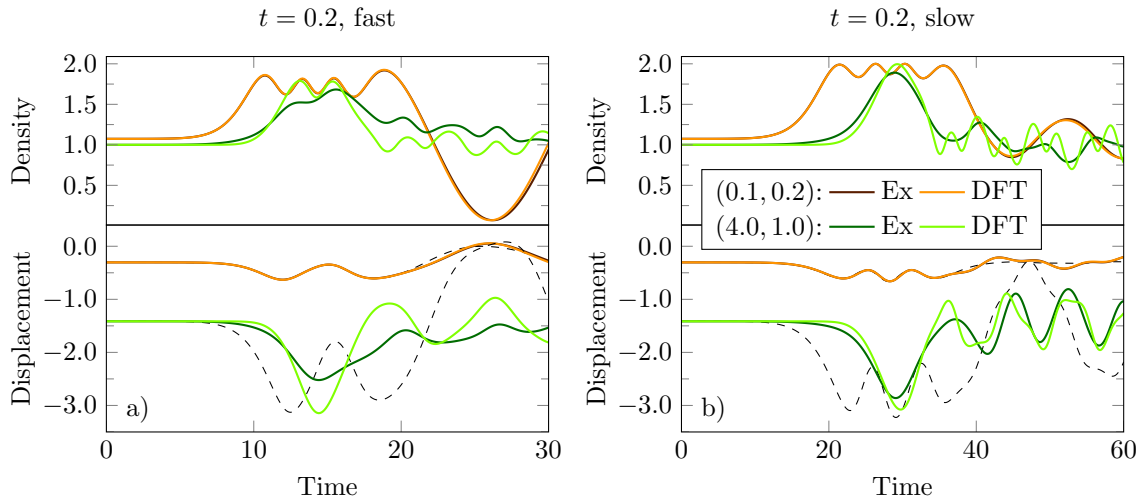

Figure 13: Electronic density and phonon displacement at the interacting site for the weakly coupled system represented by orange in figure 9 with $U = 0.1$, $g = 0.2$ and $t = 0.2$, and the intermediately coupled system represented by green in figure 10 with $U = 4$, $g = 1.0$ and $t = 0.2$. The perturbation in these panels is a Gaussian. a) has a Gaussian perturbation with amplitude 3 and full width half max (FWHM) of 7, and in b) the perturbation has amplitude 1.5 and FWHM 14. Note the different timescales of a) and b).

The system represented by orange in figure 13 has the parameters $U = 0.1$, $g = 0.2$ and $t = 0.2$ and is the same system as in figure 9, where the DFT-solution and HF-solutions were undistinguishable and in very good agreement with the exact solution. For this perturbation it can be seen how the DFT-solution is better than the HF-solution, and thus that even for weakly coupled systems the potentials from sections 2.3 actually performs better than the HF-potentials.

The system represented by green in figure 13 has the parameters $U = 4$, $g = 1.0$ and $t = 0.2$ and it is the same as in figure 10. Here we see that also for the Gaussian perturbation the DFT-solution has problems reproducing the exact solution for this systems, although it does perform better than the HF-method.

4.2 Linear Chain

The ground state of the four-site linear chain shown in figure 7b was studied for some of the different values of U and g used for the dimer presented in the previous section, and with two different external potentials. The hopping was set to $t = 1.0$ for all the simulation of this section.

Figure 14 shows the sum of the deviation in density and displacement of

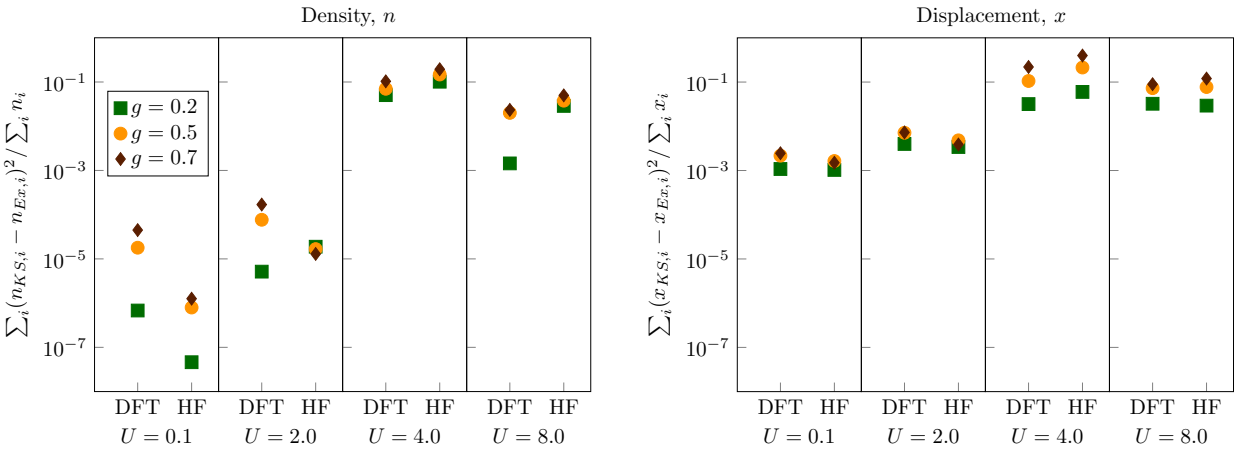

Figure 14: Total deviation squared of the DFT and HF-ground state solutions from the exact. The left panel shows the deviation in density and the right in displacement. Each subpanel indicate a different value of U and the different symbols different values of g. The external potential is $v_{ext} = [0, 5, -5, 2]$, the hopping parameter $t = 1$, and $\beta = 0.6$.

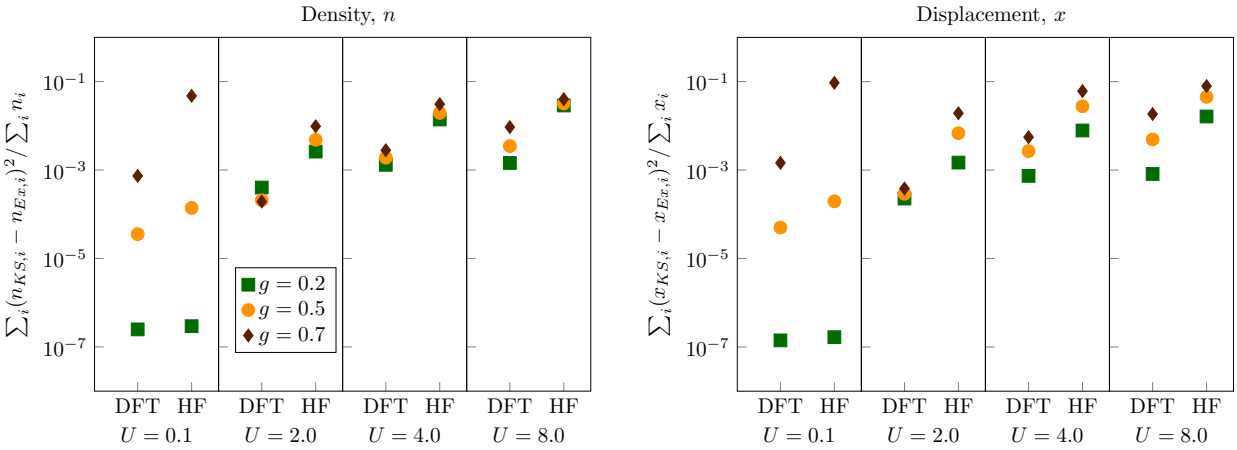

Figure 15: Total deviation squared of the DFT and HF-ground state solutions from the exact. The left panel shows the deviation in density and the right in displacement. Each subpanel indicate a different value of U and the different symbols different values of g. The external potential is $v_{ext} = U[0, 0.5, -0.5, 0.25]$, the hopping parameter $t = 1$, and $\beta = 0.6$.

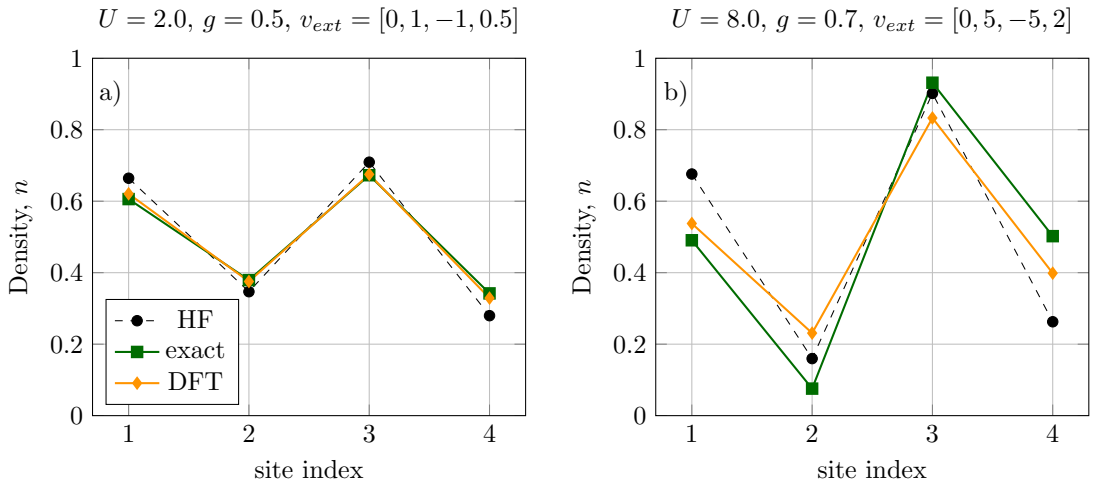

Figure 16: Here the absolute density at the different sites is shown for two of the systems shown in figure 15 and 14. Panel a) presents an intermediately coupled system with $U = 2.0$ and $g = 0.5$ for an onsite potential $v_{ext} = [0, 2, -2, 1]$. Panel b) presents a strongly coupled system with $U = 8.0$ and $g = 0.7$ for an onsite potential $v_{ext} = [0, 5, -5, 2]$

the DFT and HF-solutions from the exact solution for an external potential changing the on-site energies to $[v_1, v_2, v_3, v_4] = v_{ext} = [0, 5, -5, 2]$. Each subpanel corresponds to a different value of U, where $U = 0.1, 2.0, 4.0$ and 8.0. For each value of U three different values of g were considered, $g = 0.2, 0.5$ and 0.7.

For these systems and this particular external potential we see how the HF-potential performs better for the systems with a weak electron-electron coupling while the Hxc-potential performs better for the more strongly coupled systems.

In the next set of plots, seen in figure 15, we see the same as in figure 14 but for an external potential set relative to the electron-electron interaction, $v_{ext} = U[0, 0.5, -0.5, 0.25]$. The external potential is in other words proportional to the electronic interaction of the system, and thus varies between the different subpanels. Here it can be seen how the Hxc-potential performs consistently better than the HF-potential.

For many of the more weakly coupled systems in figure 14 the HF-potentials performs better than the Hxc-potential, something that was not observed in the previous section where the Hxc-potential performed better in all coupling regimes. Looking at the actual densities for the different systems, shown for two systems in figure 16, it can be seen that for all of the systems where the Hxc-potential performs worse than the HF-potential, the electrons are highly confined to two of the sites. Studying the performance at each specific site, it is seen that the HF-potential performs better than the Hxc-potential for densities far from half filling. This is illustrated in figure 16b), where the HF-results are closer to the exact results for the two middle sites, which are far from half-filling. The end sites, on the other hand, are close to half-filling, and here the Hxc-potential performs better. In panel a) it is clear that the HF-solution overestimates the effect of the electron repulsion, which was also observed for the dimer simulation

in the previous section.

4.3 E_{xc} and v_{xc} from the DMFT code

The DMFT code used in this project required a fair amount of computational effort to converge each data point. Therefore a small but representative set of four different combinations of parameters were chosen for study. As the exchange-correlation energy is expected to be symmetric around half-filling, data was only sampled below half-filling, save for a few points above half-filling to assure the symmetry assumption was valid.

The infinitely coordinated Bethe lattice is for the Hubbard model known to experience a Mott transition at a critical value of the electron-electron interaction $U_{c,H} = 5.88$ [5]. The Mott transition is a transition from a metallic to an insulating phase due to the appearance of a gap in the DOS, which is related to the gap in the v_{xc} [15]. The parameters chosen for study were therefore $U = 3.0$, 8.0 and $g = 0.2$, 1.0. With these values the rescaled electron-electron interactions $\tilde{U}$

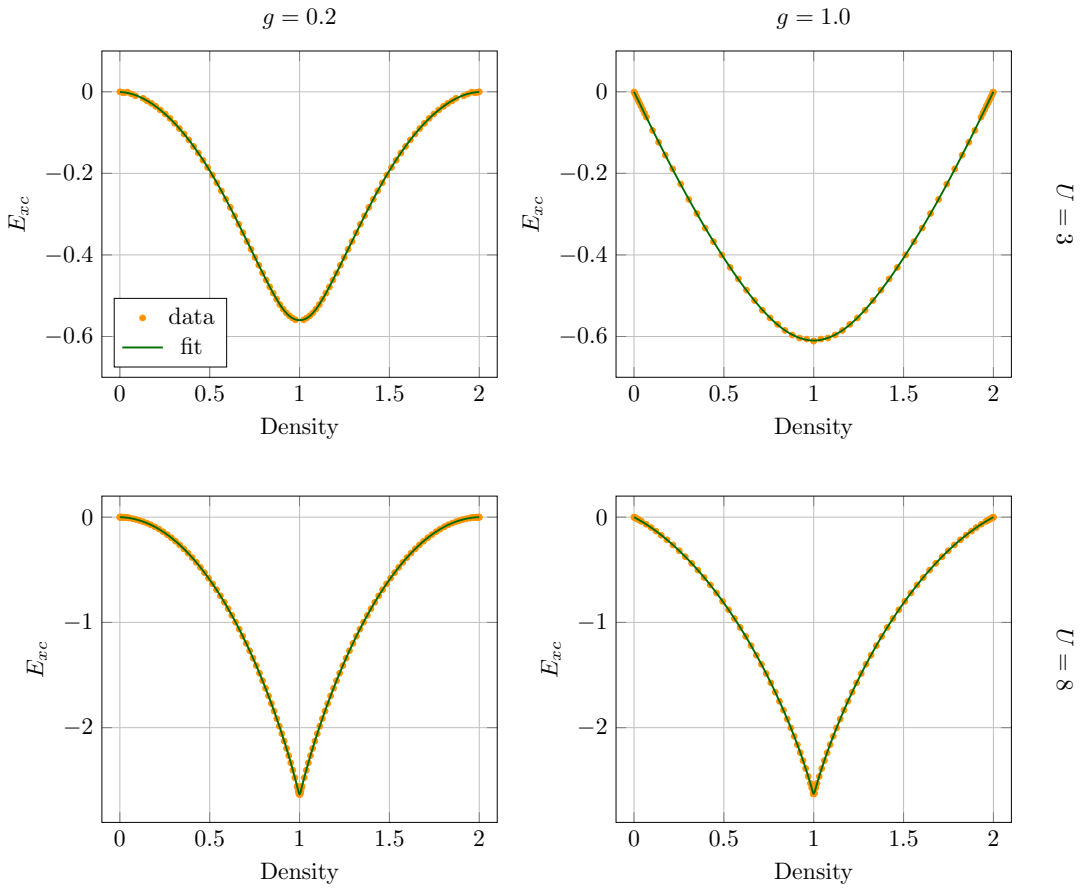

Figure 17: Exchange-correlation energies for the Bethe lattice attained with the DMFT code for $U = 3.0, 8.0$ and $g = 0.2, 1.0$. Data sampled only for densities below half-filling, data above half filling is a mirror image. The xc-energy appears to be smooth for $U = 3.0$ and discontinuous for $U = 8.0$.

were below and above $U_{c,H}$, and the weak to intermediate and strong coupling regimes are represented for both parameters U and g.

The xc-energy was extracted according to equation (65) with $x = 0$, and a fit was done to the data for each of the parameter sets. The fitting was done with a piecewise spline interpolation method which is discussed in appendix B. The interpolation method used was provided by Matlab's Curve Fitting Toolbox. The results from the fittings are shown in figure 17. In this figure it is seen how the xc-energy is smooth around half-filling for $U = 3.0$, and discontinuous for $U = 8.0$. This was expected based on the values chosen for U and g in relation to the value of $U_{c,H}$.

Comparing the two potentials for $U = 3.0$, we can see how for $g = 0.2$ the xc-energy is concave near $n = 0$, 2 while for $g = 1.0$ it is convex. This leads to a wider minima around $n = 1$ for the latter case, and will thus lead to a smoother xc-potential. The same observation can not quite be made for the energies and potentials corresponding to $U = 8.0$, as the energy is concave near $n = 0$, 2 and not smooth around $n = 1$ for both values of g. However, it is more concave for $g = 0.2$, which implies that for larger values of g the xc-energy could possibly become smooth also for values of U where it would always be discontinuous for the Hubbard model. This conclusion is in accordance with the rescaling of the effective electronic potential $\tilde{U} = U - 2g^2/\omega_0$ which is decreased for an increasing electron-phonon interaction g.

Another interesting property of these xc-energies is the slope at $n = 0, 2$. For $g = 0.2$ the curves are close to horizontal at the end points, corresponding to $v_{xc} \approx 0$. According to e.g. [15] this is indeed the case for the Hubbard model. For $g = 1.0$ however, the slope is far from 0, resulting in a non-zero v_{xc} also at $n = 0, 2$. This is in agreement with the results of section 2.3.1, where the xc-potential was found to take the value $\pm g^2/\omega_0$ at $(n - 1) = \pm 1$.

The fit of the xc-energies were then differentiated w.r.t. n, again using Matlab's Curve Fitting Toolbox, to give v_{xc}. The resulting potentials are shown in figure 18. In this figure we see how the discontinuity in the xc-energy for $U = 8.0$ gives a gap in the xc-potential, but the potentials corresponding to $U = 3.0$ are smooth. We also see how this gap for $U = 8.0$ is smaller for the larger value of g, which is in agreement with the rescaling of the effective electronic interaction $\tilde{U}$ that we saw for the analytic case.

By comparing these xc-potentials to the analytic expression from section 2.3 it is seen that the analytic expression and the DMFT-results are in good agreement at the end points for all panels but the one for $U = 3.0$, $g = 1.0$. An obvious shortcoming of the analytic potential is an underestimate of the xc-gap for $U = 8.0$.

4.4 Discussion

In this section we provide some additional discussion and reflect upon the results. We start with a comparison of the xc-potentials attained with the DMFT-code and the analytical expression derived in section 2.3. In figure 18 the DMFT-

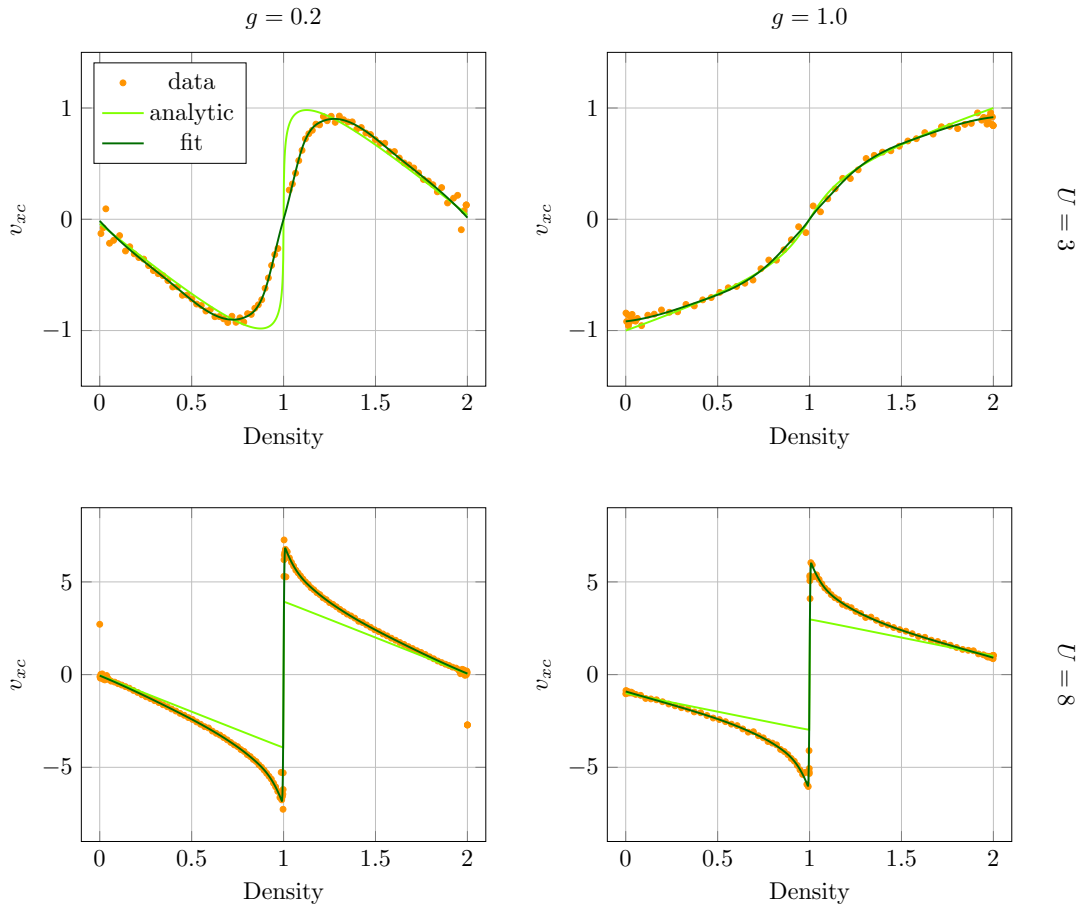

Figure 18: Exchange-correlation potentials for the Bethe lattice attained with the DMFT code for $U = 3.0, 8.0$ and $g = 0.2, 1.0$. The data points are the slope of linear regressions between the xc-energy data points. The analytical solution from section 2.3 are shown for a β which provides a good agreement.

results are presented in dark green and compared to the analytical potential shown in light green. The value of β for the analytical potentials is chosen to make it resemble the DMFT-results as well as possible. We start by noting that close to $n = 0, 2$ the slopes of the analytical and DFMT-potentials agree very well, and especially so for the cases where $U = 8.0$ and $\beta \to \infty$. Both the analytical and DMFT-potentials also have very few structural features, besides the gap at half filling. It is possible that these similarities could be attributed to the fact that both models are very local.

With increasing temperature the analytical result will more and more resemble a straight line, and thus deviate from the slope at the end points of the DMFT-result. This indicates that far from half filling $\beta \to \infty$ is always the best choice, regardless of whether the xc-potential is smooth or not at half-filling. This in turn implies that a smaller optimal β would be found in the dimer simulations for initial densities close to half-filling. This does not completely agree with the observations for the dimer, although it is true for many cases.

Then we pay some attention to the two lowermost panels of figure 18 where

we can see the potentials for $U = 8.0$. The analytical potential is shown at zero temperature, corresponding to $\beta \to \infty$, in order to reflect the discontinuity of the DFMT-results. It is seen how the DMFT-potentials are not simply linear above and below half-filling as the analytical potential, but they change quickly as they approach half-filling, ending in a peak at either side and thus show a larger gap. A similar behaviour in this area can be found for the xc-potential corresponding to the exact Bethe ansatz solution for the 1D Hubbard model, while in 3D the xc-potential does not show these peaks around half-filling [15, 12]. The 1D lattice is in fact a Bethe lattice with coordination number 2, and we could thus suspect that these peaks seen at each side of half-filling for $U = 8.0$ are possibly characteristic for the Bethe lattice.

For the two uppermost panels of figure 18, where $U = 3.0$, the potentials from the DMFT-simulations are smooth and much lower values of β are needed to resemble these potentials. However, they are still larger than the optimal values found for β during the dimer simulations.

In relation to this it can be noted that when the dimer simulations were done for $U = 8.0$, the β used, which was the β giving the initial state that most closely resembled the exact ground state, was not such that the xc-potential had a discontinuity. One explanation to this could possibly be that the chosen β gave not the global but a local minimum of the difference between the two solutions. However, before the minimization procedure was implemented β was adjusted manually, ranging from $\sim \infty$ to 0, and similar values were found for the optimal β, giving reason to believe that the found values for β do indeed give the global minimum. The two models studied in the DMFT- and analytical calculations are however two different models, which is more likely the cause of the appearance of a gap in the DMFT-potential at $U = 8.0$ while there doesn't seem to be a gap for the dimer.

When regarding the final state of the dimer simulations, the optimal β has in general changed from the one found at the start. β was not changed during the simulations, and this is not an implication that it should be changed, but an implication that using a non-infinite β does not completely account for the physics missed out by using $t = 0$ in the derivation of the analytical potential.

Another note to make on the choice of β, but for the DMFT-calculations this time, is that $\beta = 200$ might not be large enough to approximate infinity. When plotting the analytical potential for different parameters it can be seen that the smaller $\tilde{U}$ is the larger β needs to be to give a sharp step-like behaviour. If β is not large enough this would, assuming the temperature behaviour of the DMFT-results reflects the behaviour of the analytic results, mainly affect the $U = 3.0$-cases, in particular the case where $g = 1.0$. Looking at the analytical potential for these parameters and $\beta = 200$ it can be seen that although they are much more step-like than the DMFT-results, the discontinuity is not sharp. However, even though the DMFT- and analytic result are very similar in appearance, they do correspond to rather different models and the only way to deduce whether $\beta = 200$ is large enough is to run the DMFT-simulation again for other values of β and check the convergence. As mentioned previously the values of U and

g were chosen based on the Mott transition for the Hubbard model, so that $U = 3.0$ was expected to give smooth energies and potentials, while for $U = 8.0$ the potentials were expected to show a gap. As the effect of g is to reduce the effective electron-electron interaction $\tilde{U}$, the systems with $U = 3.0$ are expected to have a smooth xc-potential, and increasing β is thus not expected to cause the potentials for these systems to show a discontinuity.

5 Summary and Outlook

This section will give a brief summary on the different results attained during the course of this thesis project, as well as present some suggestions on how to proceed within the subject in the future.

In section 2.1 we have proved the HK-theorem and derived the KS-equations for the HH-model, generalizing the results of previous work. We have also derived an analytical expression for the xc-potentials of the HH-model for a single site system in contact with a heat bath of inverse temperature β and a hopping parameter $t = 0$, presented in section 2.3. The attained potential shares some features with the corresponding potential for the pure Hubbard model, but with a rescaled electron-electron interaction $\tilde{U}$ which can take negative values, and an additional term linear in $(n - 1)$. The attained expression was used in section 4.1 and 4.2 to simulate two simple systems: a dimer and a four-site linear chain, where the inverse temperature β was used as an expedient to imitate the effect of a non-zero hopping parameter. The performance of the xc-potential was compared to that of the HF-potential and to exact results. Over all it performed better than the HF-potential.

A DMFT-code was used to find the total energy of an infinitely coordinated Bethe lattice. In section 2.2 an expression was derived for the xc-energy of this system, and differentiated w.r.t n to get the xc-potential. The DMFT-simulations were run for a small but representative set of variables U and g, and the xc-energies and -potentials were extracted, presented in section 4.3.

The xc-potentials attained from the DMFT-code were compared to the analytical potentials in section 4.4. The potentials had a very similar appearance far from half filling, being linear in character. At half filling the analytical potential always experiences a discontinuity at zero temperature, while the DMFT-solutions only have a discontinuity for the systems with a strong electron-electron interaction U. Thus is because the infinite HH-Bethe lattice experiences a Mott transition in the regime between $U = 3$ and $U = 8$, while the single site system, which the analytical potential corresponds to, does not experience this transition.

Using the inverse temperature β as an expedient to amend for the shortcomings of our analytical potential, as has been done throughout this project, does not have a strict physical meaning. Another way to address these shortcomings can be found in e.g. [20] where the zero-temperature xc-potential of the Hubbard model, found in e.g. [24], is convoluted with a Lorentzian line shape to imitate spectral broadening. The result is an xc-potential which is smoothened also at zero temperature. The performance of the convoluted potential is compared to that of the potential at non-zero temperature. It is shown that the convoluted potential corresponds to a rather high temperature of the non-convoluted potential, and that it performs better. This way of smoothening the xc-potential would have a physical meaning, and it could therefore be informative to investigate the performance of an xc-potential smoothened by the convolution with a Lorentzian.

Another thing that deserves more attention is the $\tilde{U} < 0$-regime, as this is

the regime where a material would be superconducting. In reference [20] there is a discussion on the negative-U Hubbard model in a DFT-perspective. However, the presence of a negative interaction U is only assumed. A similar discussion on the HH-model would therefore be very interesting, as the rescaled electron-electron interaction of this model, $\tilde{U}$, actually can take negative values. The HH-model can thus provide a negative effective interaction on physical grounds. In this project only $\tilde{U} > 0$ has been considered save for a few cases in the small-U-regime for the dimer, where $U = 0.1$. No specific attention was paid to the fact that $\tilde{U} < 0$ in these cases however, and they did not behave in a startlingly different way from the $\tilde{U} > 0$-systems studied. By studying the conductance of the HH-model for different values of U, g and $\tilde{U}$, more insight could be gained on the significance of these regimes, e.g. as a further extension of [24] where the conductance of a single Hubbard-site coupled to leads is studied.

An approximate non-adiabatic xc-potential for a Hubbard Anderson impurity site coupled to a lead is found in [6]. The xc-potential attained there has the merit of including memory effects, and it is shown to yield better results than the potential found in [24]. It could thus be informative and interesting to do a similar investigation for a HH-site and compare to the analytical potential from section 2.3.

The perhaps most obvious way to proceed on the subject would be to use the xc-potentials that were attained from the DMFT-code. These could be used to further investigate the dimer and linear chain systems in the (A)LDA-approximation, and see if these potentials perform better than the analytical potential. Because the dimer and linear chain are one-dimensional, while the DMFT-potentials correspond to an infinite dimensional lattice, the DMFT-potentials are not expected to necessarily improve the results for these systems. Instead small systems of higher dimensionality, such as 2D or 3D, could be studied. A 3D-system would obviously be of interest as many real-life applications are concerned with three dimensional setups. However, accurate information on 2D-systems could also be of interest for practical applications, as a large group of high temperature superconductors, namely the cuprate superconductors, consists of superconducting copper-oxide layers between layers of other elements.

To study finite dimensional systems it would be ideal to use the xc-potential corresponding to systems of the corresponding dimensionality, and not the infinite Bethe lattice. These could be attained with the same approach as has been used during this project, using a different density of state during the DMFT-simulations. This has been done in [15] for the Hubbard model, and it would be interesting to compare these results for the Hubbard model to similar calculations for the HH-model. It would also be interesting to study disordered systems, that is systems with different parameter values at the different sites, as DFT is particularly suitable for disordered systems.

These are just some suggestions on what could be done in the future, and as much of the work done on the Hubbard or Holstein models separately could be interesting to generalize to the HH-model, there is lots left to discover.

References

[1] The DMFT-code used in this project was provided by Philipp Werner, Otto-von-Guericke-Universität, Magdeburg.

[2] The ED-code used in this project had been developed by Claudio Verdozzi and his group, Lund University, Lund.

[3] J. Bardeen, L. N. Cooper, and J. R. Schrieffer. *Phys. Rev.*, **108**:1175, (1957).

[4] J. G. Bednorz and K. A. Müller. *Z. Phys. B: Condens. Matter*, **64**:189, (1986).

[5] R. Bulla. *Phys. Rev. Lett.*, **83**:136, (1999).

[6] N. Dittmann, J. Splettstoesser, and N. Helbig. arXiv:1706.04547, (2017).

[7] A. L. Fetter and J. D. Walecka. *Quantum Theory of Many-Particle Systems*. McGraw-Hill, 1971.

[8] M. C. Gutzwiller. *Phys. Rev. Lett.*, **10**:159, (1963).

[9] G.-H. Gweon, T. Sasagawa, S.Y. Zhou, J. Graf, H. Takagi, D.-H. Lee, and A. Lanzara. *Nature*, **430**:187, (2004).

[10] P. Hohenberg and W. Kohn. *Phys. Rev.*, **136**:B864, (1964).

[11] T. Holstein. *Ann. Phys.*, **8**:325, (1959).

[12] M. Hopjan, D. Karlsson, S. Ydman, C. Verdozzi, and C.-O. Almbladh. *Phys. Rev. Lett.*, **116**:236402, (2016).

[13] J. Hubbard. *Proc. Royal Soc. A*, **276**:238, (1963).

[14] J. Kanamori. *Prog. Theor. Phys.*, **30**:275, (1963).

[15] D. Karlsson, A. Privitera, and C. Verdozzi. *Phys. Rev. Lett.*, **106**:116401, (2011).

[16] W. Kohn and L. J. Sham. *Phys. Rev.*, **140**:A1133, (1965).

[17] S. Kurth, G. Stefanucci, E. Khosravi, C. Verdozzi, and E. K. U. Gross. *Phys. Rev. Lett.*, **104**:236801, (2010).

[18] A. Lanzara, P. V. Bogdanov, X. J. Zhou, S. A. Kellar, D. L. Feng, E. D. Lu, T. Yoshida, H. Eisaki, A. Fujimori, K. Kishio, J.-I. Shimoyama, T. Noda, S. Uchida, Z. Hussain, and Z.-X. Shen. *Nature*, **412**:35087518, (2001).

[19] M. Levy. *Proc. Nati. Acad. Sd. USA*, **76**:6062, (1979).

[20] E. Perfetto and G. Stefanucci. *Phys. Rev. B*, **86**:081409–1, (2012).

[21] E. Runge and E. K. U. Gross. *Phys. Rev. Lett.*, **52**:997, (1984).

[22] R. T. Scalettar. Numerical Studies of Disordered Tight-Binding Hamiltonians. *AIP Conference Proceedings*, **918**:111, (2007).

[23] K. Schönhammer, O. Gunnarsson, and R. M. Noack. *Phys. Rev. B*, **52**:2504, (1995).

[24] G. Stefanucci and S. Kurth. *Phys. Rev. Lett.*, **107**:216401, (2011).

[25] W. von der Linden, E. Berger, and P. Valasek. *J. Low Temp. Phys.*, **99**:517, (1995).

[26] G. Xianlong, A-H. Chen, I. V. Tokatly, and S. Kurth. *Phys. Rev. B*, **86**:235139, (2012).

A Complementary steps for the derivation of the analytical v_{xc} for the single HH-site in section 2.3

Using the expressions in equation (67) to obtain the expectation values for x and n via the partition function given in equation (69c) we get:

$$n = 2\frac{e^{-\beta(v_s-\mu)}e^{\beta(g^2+2g\zeta)/\omega_0} + e^{-\beta(2v_s+U-2\mu)}e^{\beta(4g^2+4g\zeta)/\omega_0}}{1 + 2e^{-\beta(v_s-\mu)}e^{\beta(g^2+2g\zeta)/\omega_0} + e^{-\beta(2v_s+U-2\mu)}e^{\beta(4g^2+4g\zeta)/\omega_0}} \tag{86}$$

and

$$x = -\frac{\sqrt{2}}{\omega_0}\left[\zeta - \frac{2g(e^{-\beta(v_s-\mu)}e^{\beta(g^2+2g\zeta)/\omega_0} + e^{-\beta(2v_s+U-2\mu)}e^{\beta(4g^2+4g\zeta)/\omega_0})}{1 + 2e^{-\beta(v_s-\mu)}e^{\beta(g^2+2g\zeta)/\omega_0} + e^{-\beta(2v_s+U-2\mu)}e^{\beta(4g^2+4g\zeta)/\omega_0}}\right] \tag{87}$$

We rename $v_s - \mu = v$, $v - \frac{g^2}{\omega_0} - \frac{2g\zeta}{\omega_0} = \tilde{v}$ and $U - \frac{2g^2}{\omega_0} = \tilde{U}$ so that the expressions become somewhat simpler:

$$n(\tilde{v}, \tilde{U}) = 2\frac{e^{-\beta\tilde{v}} + e^{-\beta(2\tilde{v}+\tilde{U})}}{1 + 2e^{-\beta\tilde{v}} + e^{-\beta(2\tilde{v}+\tilde{U})}} \tag{88}$$

and

$$x(\tilde{v}, \tilde{U}) = -\frac{2\zeta}{\omega_0} - \frac{4g(e^{-\beta\tilde{v}} + e^{-\beta(2\tilde{v}+\tilde{U})})}{\omega_0(1 + 2e^{-\beta\tilde{v}} + e^{-\beta(2\tilde{v}+\tilde{U})})} \tag{89}$$

We recognize the expressions $\tilde{v}$ and $\tilde{U}$ from section 2.3 and 1.1, equation (5). The quantity $\zeta = \eta - g$ is introduced in section 2.3, where η is the phononic external potential that enters the Hamiltonian in (66).

Then we note that equation (86) looks like equation (10) and (11) of paper [26] with the substitutions $\tilde{v}_0 \to \tilde{v}$ and $U \to \tilde{U}$.

To get the inverse relation $\tilde{v}(n)$ in equation (72) we write equation (86) as:

$$n = 2\frac{z + z^2 s^{-1}}{1 + 2z + z^2 s^{-1}} \tag{90}$$

where $z = e^{-\beta\tilde{v}}$ and $s^{-1} = e^{-\beta\tilde{U}}$.

Next we multiply the above with $1 = s/s$ and move the denominator to the lhs:

$$n(s + 2zs + z^2) = 2sz + 2z^2 \to z^2 + 2zs\frac{\delta n}{\delta n - 1} + \frac{s(\delta n + 1)}{\delta n - 1} = 0 \tag{91}$$

where $\delta n = n - 1$. Solving for z and choosing the negative root for the solution gives:

$$\left(z + s\frac{\delta n}{\delta n - 1}\right)^2 = s^2\frac{\delta n^2}{(\delta n - 1)^2} - \frac{s(\delta n + 1)(\delta n - 1)}{(\delta n - 1)^2} \rightarrow$$

$$z = -s\frac{\delta n}{\delta n - 1} - s\frac{\sqrt{\delta n^2 + s^{-1}(1 - \delta n^2)}}{\delta n - 1} \tag{92}$$

Inserting the expression for z and s^{-1} from above now result in the expression:

$$e^{-\beta\tilde{v}} = e^{\beta\tilde{U}}\left(\frac{\delta n}{1 - \delta n} + \frac{\sqrt{\delta n^2 + e^{-\beta\tilde{U}}(1 - \delta n^2)}}{1 - \delta n}\right) \rightarrow$$

$$\tilde{v} = -\tilde{U} - \frac{1}{\beta}\ln\left[\frac{\delta n + \sqrt{\delta n^2 + e^{-\beta\tilde{U}}(1 - \delta n^2)}}{1 - \delta n}\right] \tag{93}$$

The expression for x is obtained by simply recognising n in equation (89):

$$x = -\sqrt{2}\left(\frac{\zeta + gn}{\omega_0}\right) \rightarrow \zeta = -\frac{x\omega_0}{\sqrt{2}} - gn \tag{94}$$

Finally expression (72) is obtained by inserting the expressions for $\tilde{v}$, $\tilde{U}$ and ζ into equation (93) and solving for $v = v_s - \mu$.

In the case of non-interacting particles, $\tilde{v} \rightarrow v$ and $\tilde{U} = 0$. Thus the KS-potential in equation (73) will explicitly look like:

$$v_{\text{KS}} = -\frac{1}{\beta}\ln\left[\frac{\delta n + 1}{1 - \delta n}\right] \tag{95}$$

B Piecewise Spline Interpolation

The interpolation of the data for E_{xc} obtained from the DMFT-code was done using a piecewise spline interpolation method from the Matlab Curve Fitting Toolbox.

A spline is a smooth function which is defined piecewise by polynomials of a given degree. Most common is the use of third degree polynomials resulting in a cubic spline. For a spline type of degree n, the continuity of the function is C^{n-1}, i.e. it can be differentiated $n-1$ times. This is achieved by requiring any adjacent polynomials to take the same value and have the same first $n-1$ derivatives. The value of the $(n-1)$th derivative in the end points must thus be given as input.

For the standard cubic spline, the second derivative is usually assumed to be zero in the end points. Upon differentiation this would result in a v_{xc} with a zero first derivative in the end points, which does not agree with neither the analytical demonstration in section 2.3 nor the actual data in section 4.3. Therefore the splines constructed for the xc-energies are of fourth order, resulting in a linear behaviour of the xc-potentials in the end points.

For each set of energy data a spline interpolation was done consisting of eight fourth order polynomials. For the energies corresponding to $U = 8.0$ a discontinuity at $n = 1$ was required. The joining points, or knots, for the polynomials were chosen to give good agreement with the data.